Summer 2020

# Freshwater Endmembers Impacting Carbonate Chemistry in the Mississippi Sound

Allison Savoie

# FRESHWATER ENDMEMBERS IMPACTING CARBONATE CHEMISTRY IN THE MISSISSIPPI SOUND

by

Allison M. Savoie

A Thesis
Submitted to the Graduate School,
the College of Arts and Sciences
and the School of Ocean Science and Engineering
at The University of Southern Mississippi
in Partial Fulfillment of the Requirements
for the Degree of Master of Science

Approved by:

Dr. Christopher Hayes, Committee Chair
Dr. Alan Shiller
Dr. Stephan D. Howden

August 2020

***Published by the Graduate School***

THE UNIVERSITY OF SOUTHERN MISSISSIPPI

## ABSTRACT

Coastal ecosystems are highly dynamic areas for carbon cycling and are likely to be negatively impacted by increasing ocean acidification. This research focused on dissolved inorganic carbon (DIC) and total alkalinity (TA) in the Mississippi Sound in order to understand the influence of local rivers that supply alkalinity to the area and buffer against ocean acidification. This area receives large fluxes of freshwater from local rivers, in addition to episodic inputs from the Mississippi River through a human-built diversion, the Bonnet Carré Spillway. Sites in the Mississippi Sound were sampled monthly during August 2018 to November 2019 and at weekly frequency during June–August 2019 in response to an extended spillway opening. Prior to the 2019 spillway opening, the contribution of the local, lower alkalinity rivers to the Mississippi Sound may have left the system more susceptible to ocean acidification during winter months, with aragonite saturation states < 2. After the spillway opened, despite a large increase in TA throughout the Mississippi Sound, aragonite saturation states remained low, likely due to hypoxia and increased $CO_2$ concentrations in subsurface waters. Throughout the study period, the Mississippi Sound generally acted as source for $CO_2$ to the atmosphere, with decreased flux after periods of increased river discharge. Increased Mississippi River input could represent a new normal in the Mississippi Sound's hydrography during spring and summer months as the spillway has been utilized more frequently in recent years. The observed fluctuations in saturation states and alkalinity conditions may be detrimental to future oyster stocks along the Mississippi coastline.

ACKNOWLEDGMENTS

I would like to thank Melissa Gilbert for analyzing the oxygen isotope samples in Dr. Alan Shiller's lab and Evan Rohde for helping run TIC/TA samples during the BCS project. Dr Xinping Hu and his lab for external calibration replicate DIC/TA samples. In addition, I would like to thank the sampling crews from USM's Division of Coastal Sciences and the Mississippi Department of Marine Resources for collecting the TIC/TA samples and in situ conductivity-temperature-depth data during the BCS project. I am grateful for the input from my committee members and advisor on this work. This research was funded by the National Science Foundation, Mississippi Department of Marine Resources, NOAA and US Environmental Protection Agency. Additionally, I would like to thank my friends and family for their constant support and motivation throughout my research.

# DEDICATION

I would like to dedicate this work to my father, Joseph Michael Savoie, who has always supported me throughout my adventures in research and life. Thank you for teaching me the value of education and hard work.

TABLE OF CONTENTS

LIST OF TABLES

LIST OF ILLUSTRATIONS

LIST OF ABBREVIATIONS

| | |
|---|---|
| *USM* | The University of Southern Mississippi |
| *DIC* | Dissolved Inorganic Carbon |
| *TIC* | Total Inorganic Carbon |
| *TA* | Total Alkalinity |
| $\Omega_{ar}$ | Aragonite Saturation State |
| *BCS* | Bonnet Carré Spillway |
| *BCH* | Beach |

# CHAPTER I - INTRODUCTION

## 1.1 Carbonate Chemistry

Increasing anthropogenic inputs of carbon dioxide ($CO_2$) from the burning of fossil fuels and deforestation have led to increases in atmospheric $CO_2$ to over 410 parts per million (ppm) as of this writing, which is more than 40% larger than pre-industrial concentrations. Approximately 30% of this anthropogenic carbon released into the atmosphere has been taken up by the world's oceans (Sutton et al. 2019). Carbon enters the ocean through short timescale processes such as air-sea exchange and long timescales such as rivers. It is removed through burial either in the form of calcium carbonate ($CaCO_3$) or as organic matter (Millero 2007). When $CO_2$ dissolves in the ocean, it is converted to carbonic acid ($H_2CO_3$) and then dissociates to a bicarbonate ion ($HCO_3^-$) and a hydrogen ion (Millero 2007; Feely et al. 2018). Bicarbonate can then dissociate to carbonate ion ($CO_3^{2-}$), which calcifying organisms will combine with calcium to form their shells out of calcium carbonate (Feely et al. 2018). The dominant carbon ion species at the ocean's current pH is $HCO_3^-$ and the second is $CO_3^2$; however, as the ocean's pH decreases there will be an overall decrease in $CO_3^{2-}$, (Pilson 2014; Logan 2010). This is due to the fact that as more $CO_2$ dissolves in the ocean, it will shift the pH down. As the pH system shifts, $CaCO_3$ shells will be more difficult for organisms to form due to the decreased amount of dissolved $CO_3^{2-}$ ions; this process is termed ocean acidification (Pilson 2014). This in turn leads to the dissolution and malformation of marine calcifier shells (Feely et al. 2018).

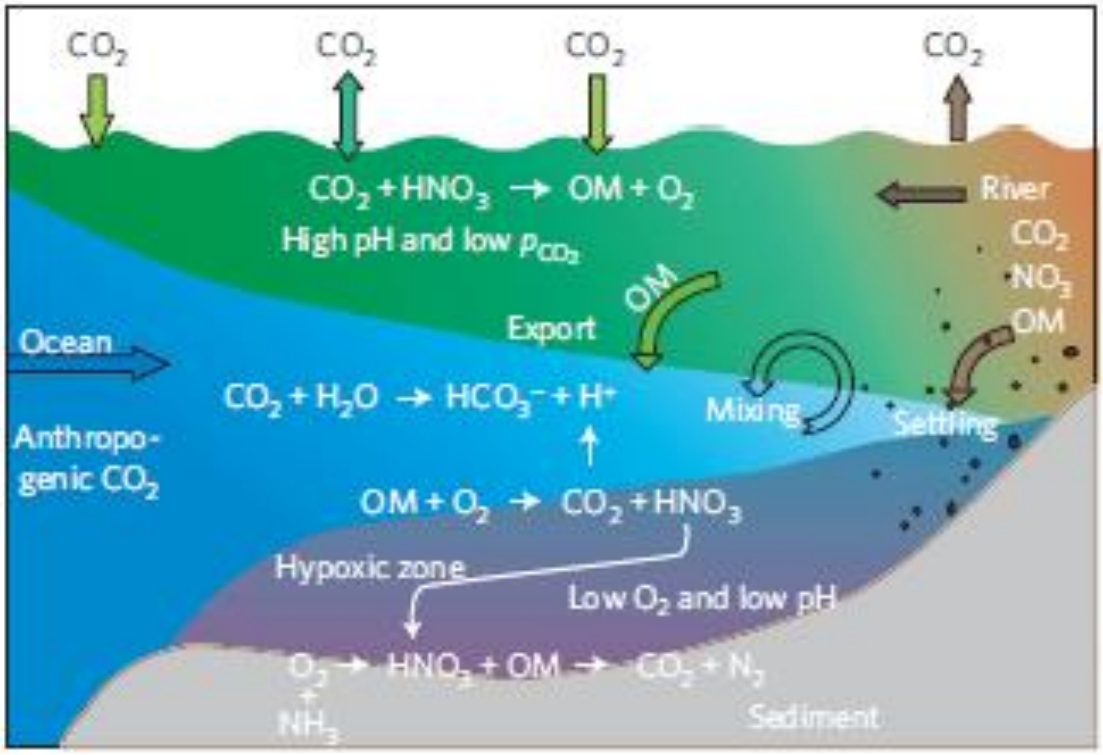


*Figure. 1.1. Conceptual model of river impacts on coastal ocean acidification*

Conceptual model that shows a large riverine export into the coastal waters that leads to eutrophication and subsurface hypoxia, which enhances subsurface ocean acidification (Cai et al. 2011).

The saturation state of surrounding waters is also an important consideration for local marine calcifiers. The saturation state of aragonite ($\Omega_{ar}$) is defined as the ion solubility product of calcium and carbonate ions, divided by the equilibrium solubility product ($\Omega_{ar} = [Ca^{2+}] [CO_3^{2-}] / K_{sp}$) (Mucci 1983; Feely et al. 2018). Water is supersaturated when $\Omega > 1$ and undersaturated when $\Omega < 1$ (Mucci 1983). However, it has been observed that many calcifying organisms need $\Omega$ values higher than 1 to continue secreting their shells (Pilson 2014; Kleypas et al. 1999). These organisms are

important because they include corals, sponges, bivalves, mollusks, and many species of plankton. All of these organisms are important for sustaining local ecosystems that support fisheries, biodiversity and ecotourism.

The inorganic carbon system was tracked in this study with measurements of dissolved inorganic carbon (DIC = $[CO_2] + [HCO_3^-] + [CO_3^{2-}]$) (Dickson 1981; Dickson et al. 2007; Millero 2007) and total alkalinity (TA). Total alkalinity is comprised of carbonate alkalinity ($[HCO_3^-] + 2[CO_3^{2-}]$) as well as the excess of other proton acceptors over proton donors present in the water at a zero level of protons at pH 4.5 ($[B(OH)_4^-] + [OH^-] + [HPO_4^{2-}] + 2[PO_4^{3-}] + [H_3SiO_4^-] – [H^+] – [HSO_4^-] – [H_3PO_4]$; Dickson, 1981; Millero 2007). Furthermore, in some coastal environments, organic anions can appreciably contribute to total alkalinity (Cai et al, 1998). Borate and sulfate terms are assumed proportional to salinity and we measured soluble reactive phosphate and silicate, according to methods in Strickland and Parsons (1972), to correct for their contribution to total alkalinity. Organic alkalinity was not estimated, although a recent study in the Mississippi-Atchafalaya estuary found organic alkalinity was less than 1% of the total alkalinity in that region (Yang et al. 2015). This study will focus on the Mississippi Sound, an estuary in the northern Gulf of Mexico. The Mississippi Sound harbors numerous public and private oyster reefs, which may be susceptible to ocean acidification.

### 1.2 Study Region

Coastal oceans are affected by a number of increasing anthropogenic stressors, including increased freshwater inputs with elevated nutrient concentrations that stimulate

phytoplankton growth (Doney 2010). Coastal areas can act as large sinks for anthropogenic $CO_2$ (McLeod et al. 2011) due to this elevated primary productivity, especially in the northern Gulf of Mexico, which receives large fluxes of freshwater and nutrients from the Mississippi River (Lohrenz and Cai 2006; Lohrenz et al. 2018). Increased primary production, in addition to stratification due to the input of low salinity waters, can induce hypoxia in subsurface waters from the degradation of organic matter, which accumulates in the sediments and in turn, can enhance local ocean acidification due the release of respiratory $CO_2$ (Fig. 1.1.; Cai et al. 2011; Laurent et al. 2017; Feely et al. 2018). Our coasts are highly dynamic and impacted by a number of stressors that should not be studied independent of one another if our aim is to understand how these systems are going to change under predicted climate change scenarios.

There has been extensive research on coastal inorganic carbon dynamics in the mid- to outer shelf region of the northern Gulf of Mexico and along the Louisiana Shelf (e.g. Cai et al. 2011; Wang et al. 2013; Feely et al. 2018), but few studies have looked at the carbon dynamics along the Mississippi inner shelf and estuaries. The Mississippi Sound is a diurnal, microtidal environment with an average salinity of 15 g/L and an average depth of 4 meters (Bianchi et al. 1999). The Mississippi Sound is separated from the Mississippi Bight by a chain of barrier islands from Mississippi to Alabama that restrict flow into and out of the Sound. Therefore, the water in the Sound generally has salinities less than 20 (on the practical salinity scale 1978) near the coast and greater than 30 near the barrier islands (Vinogradov et al. 2004). However, during times where there is increased river runoff, the Mississippi Sound waters can become much fresher and water column stratification can develop, resulting in associated hypoxia (Brunner et al.

2006; Ho et al. 2019). The Mississippi Sound is also heavily influenced by natural and anthropogenic riverine discharge (Bianchi et al. 1999). Rivers that discharge directly into this area and provide the majority of freshwater to the region include the Pearl, Wolf, Jourdan, Pascagoula, and Mobile Rivers (Table 1; Fig. 1.2). Local rivers and streams that discharge into Lake Pontchartrain can also make up about 14% of the freshwater sources to the Sound (Table 1.1). The Mississippi River can also influence this area through the Bonnet Carré spillway (BCS) (Fig. 1.2), which was constructed in order to reduce discharge through the main stem of the river during high flow conditions to protect the city of New Orleans from flooding. The Mississippi River system has much higher alkalinity and dissolved inorganic carbon compared to the local Mississippi and Alabama rivers (Cai 2003; Wang et al. 2013). This region also receives substantial rainfall, with average annual precipitation exceeding 160 cm and highest precipitation occurring from July to September, with evaporation rates around 120 cm/yr (Bianchi et al. 1999).Therefore, these varying sources of freshwater to Mississippi Sound can have very different impacts on the local carbonate chemistry.

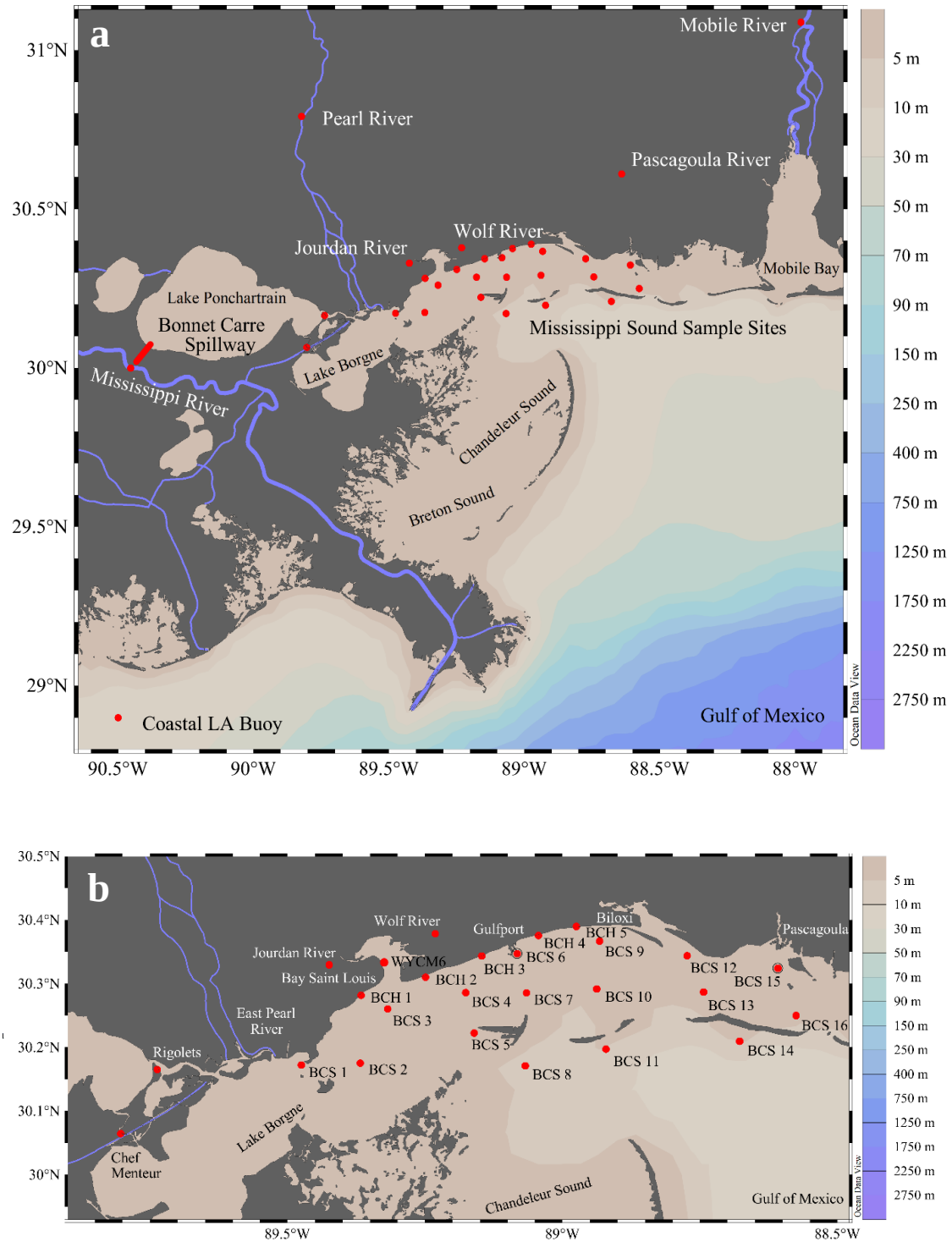


*Figure 1.2. Map of Mississippi Sound and Sample Sites*

Map of (a) study regions with all sampling stations (red circles) (b) monthly beach (BCH) sampling stations only and Bonnet Carré Spillway (BCS) sampling stations. Station WYCM6 is the location of the National Data Buoy Center's weather buoy.

The oyster fishery in the Mississippi Sound and most of the Gulf Coast states depends on the species *Crassostrea virginica* (Dugas et al. 1997), which is most abundant at salinities between 10 and 30 (Galtsoff 1964; Shumway 1996; Dugas et al. 1997). This species generally spawns during warm summer months (once water reaches ~25°C) and take ~4 months to reach sexual maturity (Hayes and Menzel 1981; Shumway 1996). During this juvenile phase, *C. virginica* shells are composed mostly of aragonite until they form their thicker, primarily calcite-based shells as adults and are thus more sensitive to changes in pH during their early life stages (Lee 1990; Lemasson et al. 2017). For instance, laboratory studies have shown *C. virginica* to have decreased calcification rates around $\Omega_{ar} = 1.4$ (Ries et al. 2016). This means that *C. virginica* juveniles that use amorphous $CaCO_3$ or aragonite are more susceptible to ocean acidification than adults that tend to form calcite shells (Lemasson et al. 2017). Therefore, in addition to understanding how large fluxes of freshwater affects local carbonate chemistry throughout the year, it is important to understand when these fluxes occur relative to the oyster spawning season. Understanding how multiple stressors (i.e., increases in freshwater, eutrophication, and hypoxia) affect ocean acidification in each region is important for informing local stakeholders on how to best conserve coastal ecosystems that provide fishery and recreational revenue. As an example of an estuary with increasing freshwater inputs, insights from this study of the Mississippi Sound will

contribute to predictions of coastal acidification stressors worldwide. Coasts are highly dynamic and impacted by a number of stressors that should not be studied independent of one another if our aim is to understand how these systems are going to change under predicted climate change scenarios.

Table 1.1

Annual Mean Input of Freshwater Sources to the Mississippi Sound

| Freshwater Sources to the Mississippi Sound | Annual Mean Input | Percent Contribution to MSS | Reference |
|---|---|---|---|
| All rivers and streams debouching into Lake Pontchartrain | 188 $m^3/s$ | 14 | Sikora & Kjerfve 1985 |
| Pearl River | 362 $m^3/s$ | 28 | Kjerfve 1983 |
| Wolf and Jourdan Rivers | 41 $m^3/s$ | 3 | Eleuterius & Beaugez 1979 |
| Biloxi, Tchoutacabouffa Rivers and Bernard and Old Fort Bayous | 29 $m^3/s$ | 2 | Kjerfve 1983 |
| Pascagoula River | 408 $m^3/s$ | 31 | Kjerfve 1983 |
| Mobile Bay Outflow Pass Aux Herons | 277 $m^3/s$ | 21 | Schroeder et al. 1990; Schroeder 1978 |
| Total Directly into MSS | 1305 $m^3/s$ | | |

### 1.3 2019 Bonnet Carré Spillway Opening

As mentioned in section 1.2, the Mississippi River can influence this area through the Bonnet Carré spillway (BCS), a human built diversion connecting the Mississippi River to Lake Pontchartrain. When the BCS is open, it allows up to 7,079 $m^3/s$ of Mississippi River water to discharge into the Lake Pontchartrain estuary

(https://www.mvn.usace.army.mil/Missions/Mississippi-River-Flood-Control/Bonnet-Carre-Spillway-Overview/Spillway-Operation-Information/ accessed 05/10/2020). The water then flows through the Rigolets and Chef Menteur Pass out of Lake Pontchartrain toward the Mississippi and Chandeleur Sounds over a 4 to 5 week period (Parra et al. 2020). Historically, the opening of this spillway has resulted in large fluxes of freshwater to the Mississippi Sound that have led to widespread oyster reef mortality (Posadas 2019).

The BCS was opened for a record number of days during our study period in summer 2019 and this was the first time that it was opened twice in one year; opening occurred from February 27 to April 11 and May 10 to July 27 (https://www.mvn.usace.army.mil/Missions/Mississippi-River-Flood-Control/Bonnet-Carre-Spillway-Overview/Spillway-Operation-Information/ accessed 05/16/2020). The 2019 spillway opening had devastating impacts to the local fisheries and recreational economy along the Mississippi coast. The Mississippi Sound region serves as an important ecosystem for the oyster fishery for the state, with the majority of oyster landings for the state of Mississippi coming from the western Sound (Dugas et al. 1997). The opening of the BCS led to the loss of local oysters, closing of beaches from harmful algal bloom presence, widespread hypoxia, and the stranding of numerous dolphins and turtles (https://gcrl.usm.edu/news/2019.bonnet.carre.spillway.overview.php accessed 05/16/2020). Therefore, this event gave us the opportunity to study how multiple stressors (i.e. increased freshwater, eutrophication, and hypoxia) can affect local carbonate chemistry.

## 1.4 Objectives

The primary objective of this research was, first, to establish an annual time-series of the inorganic carbon system from August 2018 to November 2019, with spatial coverage across the Mississippi Sound from Waveland to Biloxi. This study provides a yearlong time-series of data on carbon dynamics in a region of the northern Gulf of Mexico that has few historical measurements. In addition, we investigated how the local rivers affect carbonate chemistry in the Mississippi Sound. With this data, we infer the susceptibility of the area to future ocean acidification and determine when Mississippi Sound is a source or sink of $CO_2$ from the atmosphere. We predict that our time series data from the MS Sound will show that the area will likely serve as a sink for $CO_2$ during winter and spring months during lower temperatures and peak primary production. Then, as the waters in the Sound begin to retain more heat during summer and fall months, the system will act as a net source for $CO_2$. We further assess whether DIC and TA are being added or removed in MS Sound throughout the year. Due to a substantial freshwater flux from the BCS between February and July 2019, we describe how the introduction of freshwater from the Mississippi River, which has a much higher DIC and TA than local rivers, impacts the dissolved inorganic carbon system in the Mississippi Sound and how long it takes for the system to recover from the event. We predict that the MS Sound will likely have more acidic conditions that favor shell dissolution during the fall and winter months of our time series data due to increased dissolved $CO_2$ from elevated organic carbon respiration in the fall and cooler water temperatures in the winter that can take up more $CO_2$. During spring and summer months, it is more likely that we will have conditions that favor shell formation, especially when the Sound is receiving higher

volumes of MS River water that tends to have much higher alkalinity than the local rivers.

In addition, the magnitude of the flux of Mississippi River water that actually made it to the Mississippi Sound was unknown in previous years that it has been opened. The magnitude of Mississippi River water that reaches the Sound likely varies greatly between opening events depending on daily discharge through the BCS and length of opening. However, this study was able to use a three endmember mixing model in order to calculate the fraction of Mississippi River water in the Sound and estimate the impact on the region based on this opening event. By understanding how our region is impacted by increased freshwater and the subsequent eutrophication and hypoxia, we are better equipped to assess ocean acidification impacts to these coastal regions in the future.

# CHAPTER II – METHODS

## 2.1 Beach Sampling

Beach stations ("BCH" stations) were sampled, weather and environmental conditions permitting, approximately monthly from August 2018 to November 2019 (Fig. 1.2b). Sampling methods and sample analysis for the monthly DIC and TA measurements followed standard protocols described in Dickson et al. (2007) with some amendments due to site conditions. Samples collected from five BCH pier locations (Fig. 1.2b) were collected with gloved hands by triple rinsing a 500 mL Nalgene wide-mouth HDPE bottle with site water and then completely filling the sample bottle. The samples were then stored dark, on ice in a cooler and placed out of direct sunlight, while they were transported back to the laboratory. Once in the laboratory, the samples were filtered with 0.45 µm Whatman Puradisc polypropylene syringe filters into a 250 mL glass container and each sample was poisoned with 50 µL of a 50% saturated reagent grade $HgCl_2$ solution. The bottle was inverted several times to disperse the $HgCl_2$ and then samples were stored in the dark, at room temperature (~22°C) and analyzed the following day.

Nutrients for BCH samples were collected in acid washed 250 mL Nalgene bottles utilizing the protocol outlined in Shiller (2003). Briefly, the acid-cleaned bottle was attached to a nonmetallic pole to collect the water sample. The bottle was rinsed three times and filled by a sampler wearing polyethylene gloves. After collection, samples were stored on ice until returned to the laboratory, where samples were filtered through acid washed 0.45 µm Whatman Puradisc polypropylene syringe filters into 125 mL acid washed brown Nalgene bottles after one filtrate rinse. Samples were then frozen

until analysis on a SEAL Auto Analyzer (AA3 HR) for dissolved silicate and soluble reactive phosphate.

### 2.2 Bonnet Carré Spillway Sampling

Bonnet Carré Spillway (BCS stations; Figure 1.2b) response samples were collected on a weekly basis from the Mississippi Sound from June to August 2019 from two small boats, where one boat sampled stations 1 to 8 and the second sampled 9 to 16. Samples were collected at the 16 stations throughout the Mississippi Sound and Bight using Niskin bottles at 0.5 m below the surface and 0.5 m above the bottom (Fig. 1.2b). For DIC and TA samples, a glass 250 mL Pyrex bottle was triple rinsed with sample water and then filled smoothly and completely. Following collection, the headspace was adjusted by removing seawater so that 1% of the bottle volume is left to allow for water expansion (i.e., 2.5 mL headspace for a 250 mL bottle). The samples were poisoned with 50 microliters of 50% saturated reagent grade $HgCl_2$ solution once the boats returned to the shore, capped tight, stored in a cooler for transportation and then in a refrigerator until analysis (usually within 3-5 days).

Nutrients for BCS samples were collected in precleaned and acid washed (10% HCl) 1 L HDPE samples bottles that were rinsed with DI water then rinsed three times with sample water before being filled and stored on ice until return to the laboratory. Samples were filtered through pre-combusted glass fiber filters (Whatman GF/F) and the filtrate was collected in pre-cleaned, acid washed brown 60 ml HDPE bottles after three filtrate rinses and then frozen until analysis for soluble reactive phosphate and dissolved silicate.

## 2.3 River and Pass Sampling

Samples were also collected from seven rivers and estuarine sites in Alabama, Mississippi, and Louisiana to constrain river endmember values for DIC and TA (Fig. 1.2a). The rivers include Wolf, Jourdan, Pascagoula, Mobile, Mississippi, Pearl and East Pearl Rivers. The Mississippi and Pearl Rivers were sampled once in June and July 2019 and the rest of the rivers were sampled only once in June 2019. The estuarine sites are passes from Lake Pontchartrain to the Mississippi Sound called the Chef Menteur Pass and The Rigolets. The passes were sampled 8 times from July to August 2019. The samples were collected, transported, and processed according to the procedure outlined for the BCH samples (section 2.1), with the exception that they were not filtered.

## 2.4 Chemical and Statistical Analysis

Samples were analyzed for inorganic carbon using methods from Dickson et al. (2007) by acidifying 30 mL of sample with 4 mL of 2 M phosphoric acid and measuring the extracted $CO_2$ on a UIC Coulometer. Samples were analyzed for total alkalinity (TA) by Gran Titration (Gran 1952) on an Apollo SciTech Alkalinity Titrator on the day following DIC analysis. Samples were brought to 24°C using a water jacket before both DIC and TA analysis. The BCS samples were unfiltered, while the monthly beach samples were filtered. Therefore, we use the term total inorganic carbon (TIC) for BCS samples and DIC for BCH samples. To determine the effect of filtration on TA and DIC for the BCH samples, a filtered and unfiltered sample were collected in November 2017 at all five beach locations (Fig. 1.2b). One set of beach samples was filtered according to the methods described in the BCH Sampling locations and techniques; while the

duplicate set of samples was not filtered, although all other methodology remained the same between the two sample sets. We were able to conclude that for both TA and DIC the filtered versus unfiltered samples were not statistically significant (single factor ANOVA, $p$=0.99 for TA and $p$=0.87 for DIC) (Table 2.1).

Table 2.1

Measured TIC and TA for filtered and unfiltered samples collected at BCH stations November 13, 2019

| Station | Filtered TIC (µmol/kg) | Unfiltered TIC (µmol/kg) | Filtered TA (µmol/kg) | Unfiltered TA (µmol/kg) |
|---|---|---|---|---|
| BCH 1 | 1315 | 1329 | 1359 | 1346 |
| BCH 2 | 1787 | 1783 | 1977 | 1980 |
| BCH 3 | 1750 | 1873 | 2052 | 2052 |
| BCH 4 | 1642 | 1645 | 1830 | 1831 |
| BCH 5 | 1505 | 1481 | 1636 | 1636 |

Our methods were intercalibrated using Dickson Seawater Standards for data quality assurance and control. For DIC samples, all samples were analyzed only once on the coulometer to minimize uncertainties related to gas exchange; however, by repeat measurements of the Dickson's seawater standard, the relative standard deviation of DIC measurements on this instrument is ± 1%. All TA samples were analyzed in duplicates or triplicates to achieve a precision of roughly 20 µM, which equates to ~1% relative standard error for seawater and up to 5% for fresher samples. The relative standard deviation from repeat measurements of Dickson's seawater standards for TA on this instrument was ± 0.1%. The DIC and Alkalinity measurements were externally intercalibrated by analyzing replicate samples with Dr. Xingpeng Hu's laboratory at

Texas A&M University Corpus Christi. Replicate water sample analyses (n = 9) from the location of the Coastal Louisiana (LA) PMEL buoy (Fig. 1.2a) agreed within 0.6% for DIC and 0.4% for alkalinity.

The partial pressure of $CO_2$ of the water ($pCO_{2(water)}$) and aragonite saturation state ($\Omega_{ar}$) were calculated using the CO2SYS program (Pierrot et al. 2006). The set of constants used for this analysis for K1 and K2 were from Lueker et al. (2000), $KHSO_4$ from Dickon (1990), KHF from Perez and Fraga (1987), and $[B]_I$ from Lee et al. (2010). The chosen pH scale was the total scale (mol/kg of seawater). Error propagation for $pCO_2$ and $\Omega_{ar}$ was determined using the CO2Sys Excel program software developed by Orr et al. (2018). TIC/DIC and TA data were compiled into the CO2SYS program along with *in situ* salinity, temperature, pressure, and measured concentrations of dissolved phosphate and silicate. The calculated $\Omega_{ar}$ values had an average propagated uncertainty of 18%. The calculated $pCO_{2(water)}$ values from the samples were used along with the calculated partial pressure of $CO_2$ of the air ($pCO_{2(air)}$) obtained from PMEL's Coastal LA buoy (Fig.1a) that measures the fraction of $CO_2$ in air ($xCO_{2(air)}$) throughout the year. The calculated $pCO_{2(water)}$ values had an average propagated uncertainty of 22%. The $pCO_{2(air)}$ estimates, based on $xCO_2$ measurements from the $MAPCO_2$ system used by the Coastal LA PMEL buoy, have an uncertainty of <0.2% (Sutton et al. 2014). Using this data, we calculated $pCO_{2(air)}$ using the equation:

$$pCO_{2\,(air)} = xCO_{2\,(air)}\,[P_{baro}-P_{sw}], \quad (1)$$

where $P_{baro}$ is the barometric pressure obtained from the buoy and $P_{sw}$ is the surface seawater vapor pressure at the measured sea surface temperature and salinity from each

station (Weiss and Price 1980). Using the calculated $pCO_{2(air)}$, the flux of $CO_2$ ($FCO_2$) into or out of the Sound was calculated using the equation:

$$FCO_2 = k\ K_0\ [pCO_{2(water)} - pCO_{2(air)}], \quad (2)$$

where, k is the gas transfer velocity of $CO_2$ using the equation from Wanninkhof (1992),

$$k = 0.31 u_{10}^2 (Sc^*)^{-1/2}, \quad (3)$$

where $u_{10}$ is the wind speed calibrated to 10 m above the surface using the equation:

$$u_{10} = u_1 (z_2/z_1)^P, \quad (4)$$

where $u_1$ is the daily averaged wind speed for each sampling date obtained from the National Data Buoy Center's Station WYCM6 near the Bay Waveland Yacht Club, MS (Fig. 1), $z_2$ is 10, $z_1$ is 5, and P is a constant 0.11 (Hsu et al. 1994). The reported accuracy of wind speed measurements at WYCM are 1.0 m/s (https://www.ndbc.noaa.gov/rsa.shtml accessed 06/17/2020). The Schmidt number (Sc*) is calculated from kinematic viscosity divided by molecular diffusivity of $CO_2$ in water (Wanninkhof 1992; Wanninhkof and McGillis 1999). $K_0$ in Eq. 2 is the solubility coefficient of $CO_2$ at the in situ temperature and salinity (Weiss 1974). The reported uncertainty in k is 30% (Wanninkhof 1992) and the uncertainty in $K_0$ is 0.2% (Weiss 1974). The resulting median for the propagated relative error in the flux calculations was 48%.

The fraction of Mississippi River water was calculated by a linear mixing model using oxygen isotopes in water and salinity (M. Gilbert unpubl., Sanial et al., 2019). Essentially, the oxygen isotopes in $H_2O$ from the Mississippi River, seawater and the local Mississippi/Alabama rivers are distinct; thus, using a three end-member linear mixing model, fractions of water from these three sources were derived. Using this data,

we also calculated predicted TA and TIC values at the BCS surface stations based on the contribution of each endmember and the measured endmember values (Table 3.1). The local river freshwater endmember was a weighted average for each month (June, July and August) depending on measured discharge from available USGS data for the Pearl, Wolf, Pascagoula, and Mobile Rivers (no discharge data was available for Jourdan River). Statistical data from this study was completed using linear regression analysis from Microsoft Excel. All p-values provided are at the 99% confidence interval.

# CHAPTER III – 2019 BONNET CARRÉ SPILLWAY OPENING

## 3.1 Bonnet Carré Spillway Effective Freshwater Endmembers

TIC and TA showed a positive correlation with salinity (respectively, $r = 0.83$, df = 347, $p < 0.01$; Fig. 3.1a and $r = 0.84$, df = 348, $p < 0.01$; Fig. 3.1b); these correlations do not include the river and seawater endmember data. This correlation between TA and salinity indicates that TA distribution was mostly conservative for our study region during the BCS opening. However, TIC had a lower correlation coefficient and, thus, behaved less conservatively in this area (Fig. 3.1a). The comparison of predicted TA, based on the water isotope mixing model assuming freshwater TA endmembers mentioned in Sec. 2.4, with the measured TA for the BCS surface samples also indicated that TA for this region behaved mostly conservative. There was some removal of TA, likely due to biological uptake, resulting in a linear regression lower than the 1:1 line (Fig. 3.2b). Predicted TA had a root mean square error of 9.7 μmol/kg, which is about 1% of the average TA observed. TIC behaved less conservatively, with the data being more scattered when comparing the calculated and measured TIC (Fig. 3.2 a). This indicates more biological influence on the data, likely from primary production and respiration. The root mean square error for predicted TIC was 52 μmol/kg, or about 5% of the average observed TIC. The data from the BCS sampling determined a freshwater TIC effective endmember (derived from the y-intercept of a simple linear regression between TA and salinity) of 1,193 ± 23 μmol/kg and a freshwater TA effective endmember of 1,276 ± 24 μmol/kg (Fig. 3.1a & b). Therefore, while the BCS was open the effective TA endmember fell between the measured values for the Mississippi River and Mobile River, with lower values from station 1 that were similar to the measured Pearl River

endmember (Fig 3.1b; Table 3.1). While the simple (Model I) linear regression was used assuming salinity is an independent variable, similar conclusions are reached about the apparent freshwater endmembers using a Model II type linear regression which assumes both salinity and TA are dependent variables (e.g., 1162 ± 25 μmol/kg for effective TA endmember using Model II regression).

Table 3.1

River Endmember Data for TA and TIC

| River Endmember Data for Total Alkalinity and Total Inorganic Carbon | | | | | |
|---|---|---|---|---|---|
| **Rivers** | **Latitude** | **Longitude** | **Sample Date** | **TA (μmol/kg)** | **TIC (μmol/kg)** |
| Mississippi | 29.9997 | -90.4538 | 6/26/2019 | 2421 | 2426 |
| | | | 7/18/2019 | 2448 | 2420 |
| Pearl | 30.7919 | -89.8225 | 6/27/2019 | 530 | 549 |
| | | | 7/18/2019 | 288 | 532 |
| East Pearl | 30.4624 | -89.6948 | 6/27/2019 | 179 | 473 |
| Jourdan | 30.3296 | -89.4244 | 6/25/2019 | 396 | 441 |
| Wolf | 30.3784 | -89.2318 | 6/25/2019 | 87 | 240 |
| Pascagoula | 30.611 | -88.6410 | 6/25/2019 | 189 | 392 |
| Mobile | 31.0879 | -87.9784 | 6/25/2019 | 861 | 817 |

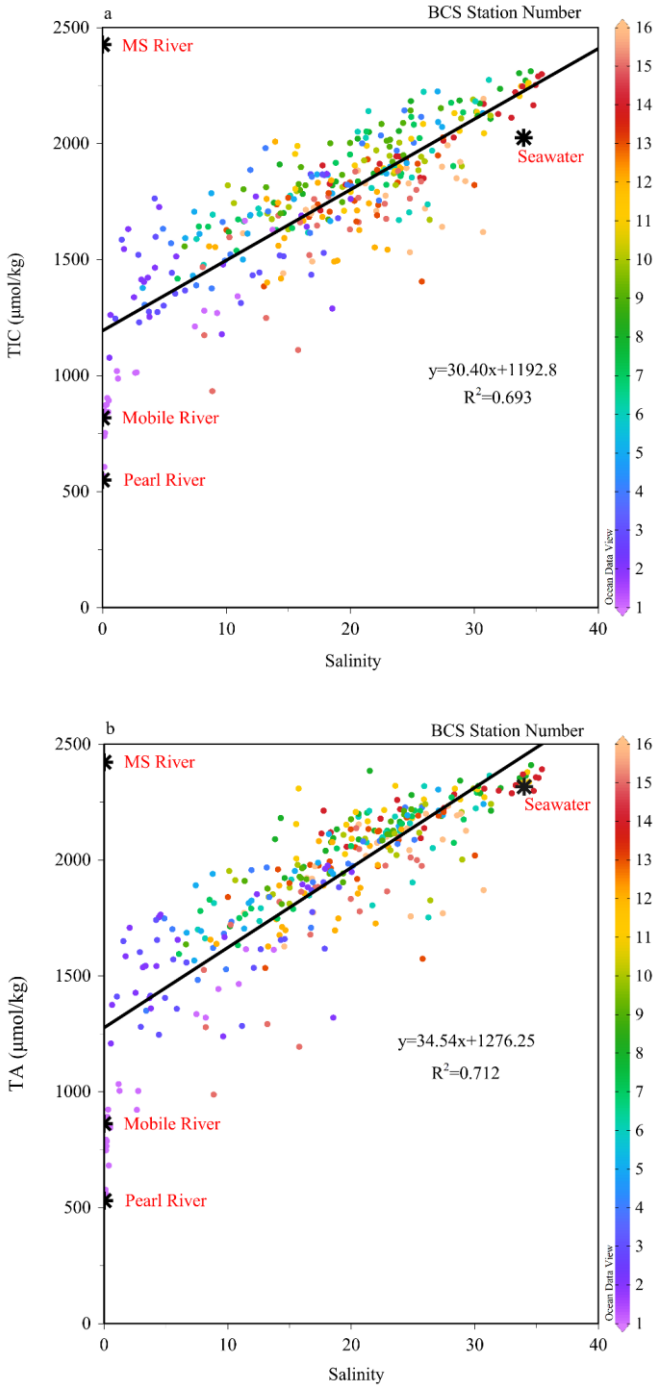


*Figure 3.1. Bonnet Carré Spillway sample effective TIC and TA endmembers*

(a) TIC (µmol/kg) and (b) TA (µmol/kg) from surface and bottom BCS samples. Black stars indicate measured endmembers (labeled with individual rivers) and were not included in the linear regression and statistical calculations.

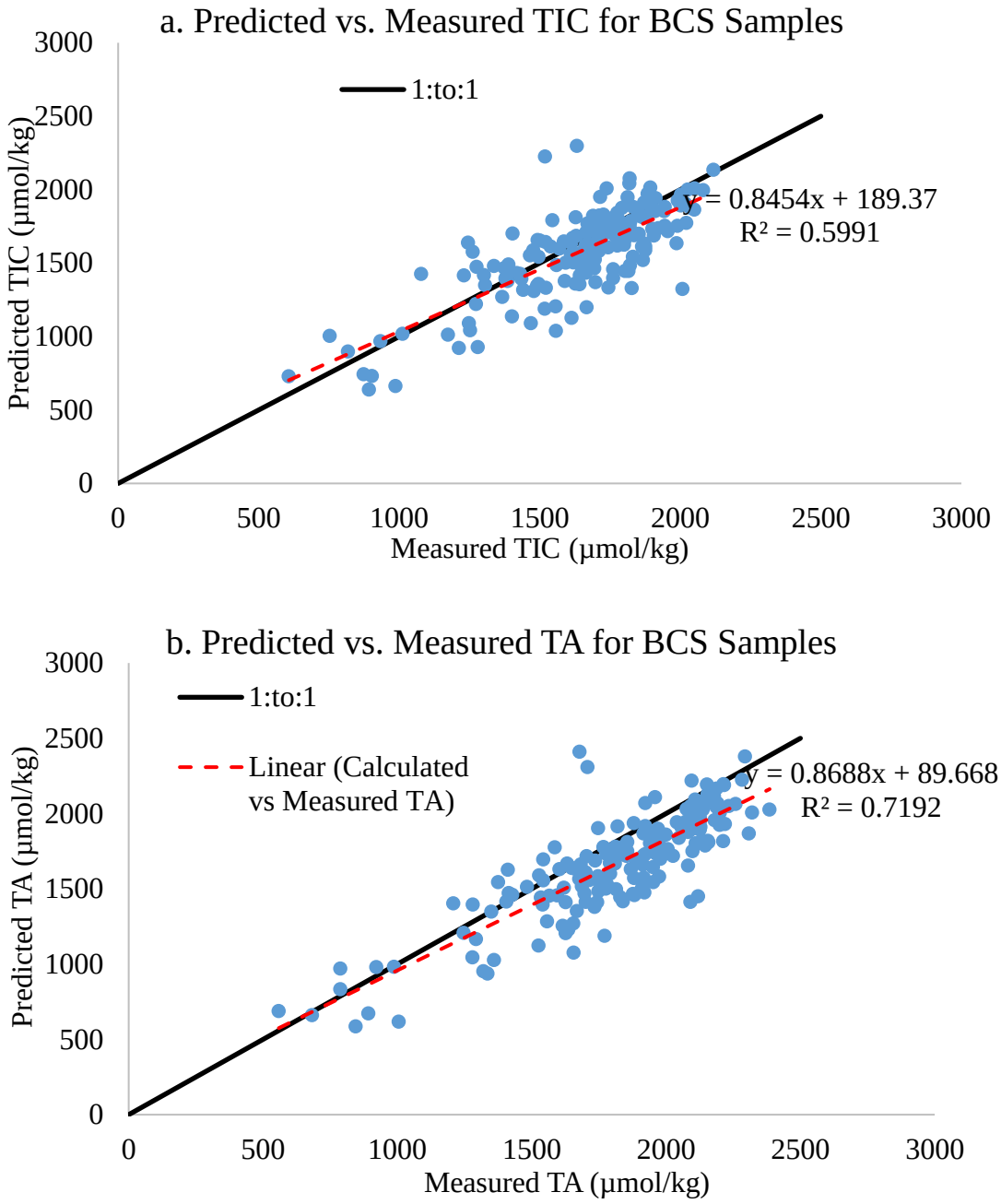


*Figure 3.2. Comparison of calculated TIC with measured TIC and calculated TA with measured TA for the BCS samples*

Comparison of (a) predicted total inorganic carbon (TIC) (µmol/kg) with measured TIC and (b) predicted total alkalinity (TA) (µmol/kg) with measured TA for the BCS samples. Predicted TA and TIC were calculated using measured freshwater endmember values and

the fraction of MS River, local river, and seawater at each station calculated with the freshwater endmember mixing model.

### 3.2 Bonnet Carré Spillway Influence on Passes

The Rigolets and Chef Menteur Pass were sampled eight times in total during the summer of 2019. During the first five weeks of sampling from late June to early August, the salinity remained below 1 for both sites (3.3a) However, on the August 14 sampling, The Rigolets had an increase in salinity to over 3, while the Chef Menteur Pass had a delayed increase on August 22 and only went up to ~1.8 (Fig. 3.3a). TIC and TA followed the opposite trend with a general decrease throughout the summer (3.3b & c). These fresh, high TIC/TA values until the end of July are likely indicative of the Mississippi River water from the BCS. Once the BCS had closed on July 27, the straits began to decrease in TIC and TA (Fig, 3.3b & c).

a. Salinity of Passes During Summer 2019

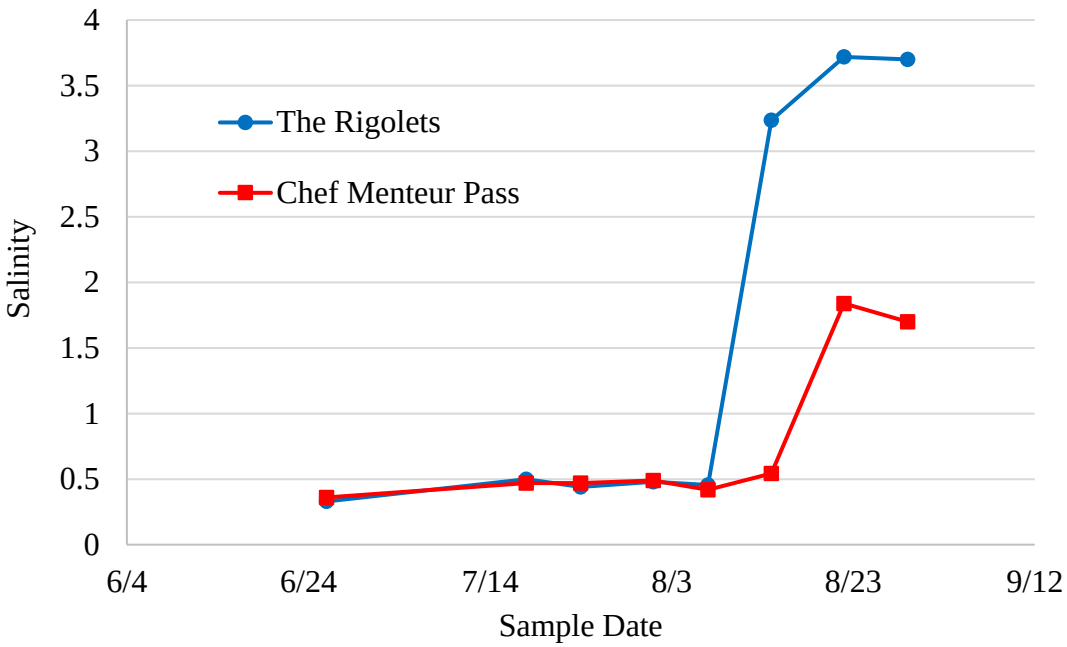


b. TIC (µmol/kg) of Passes During Summer 2019

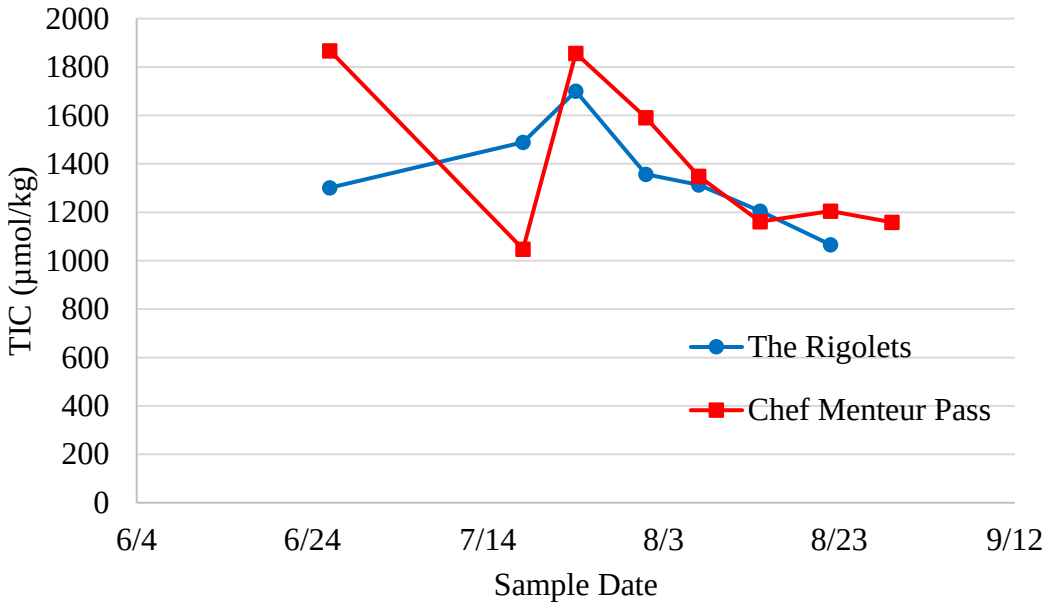

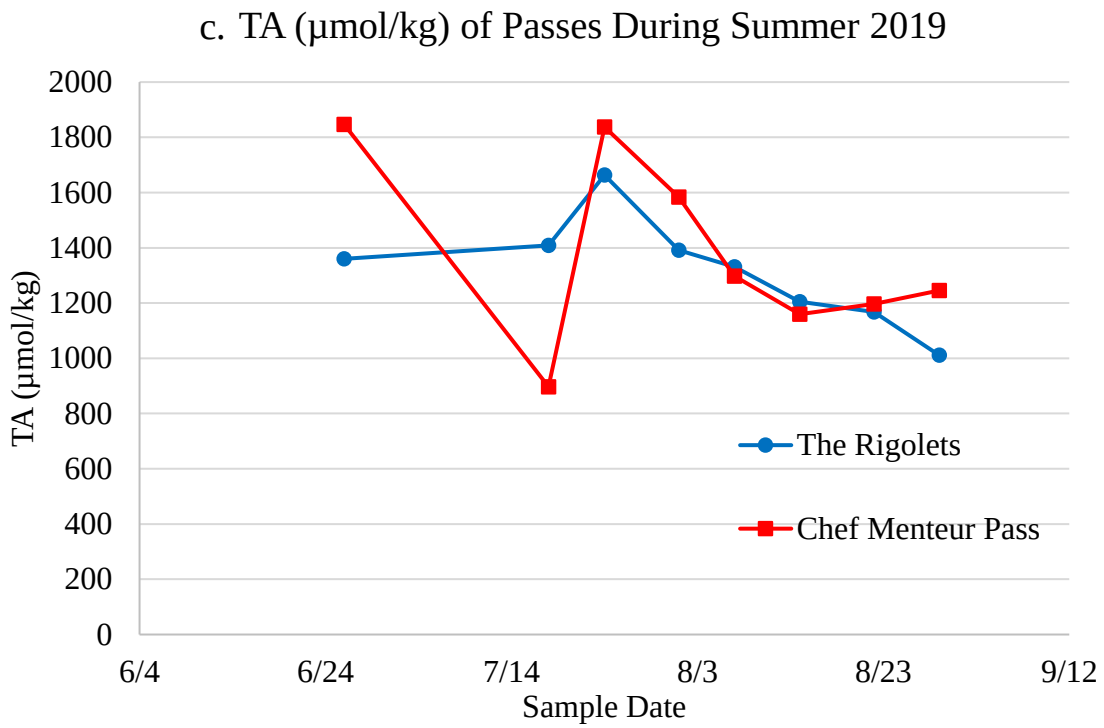


*Figure 3.3. Measured salinity, TIC, and TA through the Rigolets and Chef Menteur Pass during summer 2019*

(a) Salinity, (b) total inorganic carbon (TIC) (µmol/kg), and (c) total alkalinity (TA) (µmol/kg) collected from The Rigolets (blue circles) and Chef Menteur Pass (red squares) during summer 2019.

### 3.3 Bonnet Carré Spillway Surface Data

To determine what freshwater sources are influencing the Sound, we used the linear endmember mixing model, previously described, to deconvolve the relative amount of local river input (from Mississippi and Alabama rivers) and Mississippi River input. Our results indicate surface water in the western Mississippi Sound received larger contributions of Mississippi River water while the BCS was open, excepting station BCS 1, which, as previously mentioned, was primarily influenced by the Pearl River outflow

(Fig. 3.4). From late June to mid-July, the majority of the freshwater present at each station was sourced from the Mississippi River in comparison to local river sources (Fig. 3.4b). After the BCS closed, the plume of Mississippi River water moved eastward through the Sound until it dissipated about a month after the closure (Fig. 3.4). Similarly, salinity measurements indicate the same expansion of the plume of Mississippi River water while the BCS was open. The recovery of the Sound was indicated by increasing surface salinities during the 3 weeks following the closure of the BCS (Fig. 3.5a). Saturation states ($\Omega_{ar}$) were reduced in the western Sound and at stations closest to the coast (i.e., 9, 12, and 15) (Fig. 3.5d). The $\Omega_{ar}$ began to increase in surface waters throughout the Sound approximately one month after the BCS had closed (Fig. 3.5d). TIC and TA had a similar patterns; however, they both remained fairly high across the Sound, with the exception of BCS station 1 having the lowest observed TIC and TA (Fig. 3.5b & c), due to the influence of the Pearl River (Fig. 3.4). Coastal stations also had lower TA compared to the rest of the Sound, which could have resulted from local river influence (Fig. 3.5c).

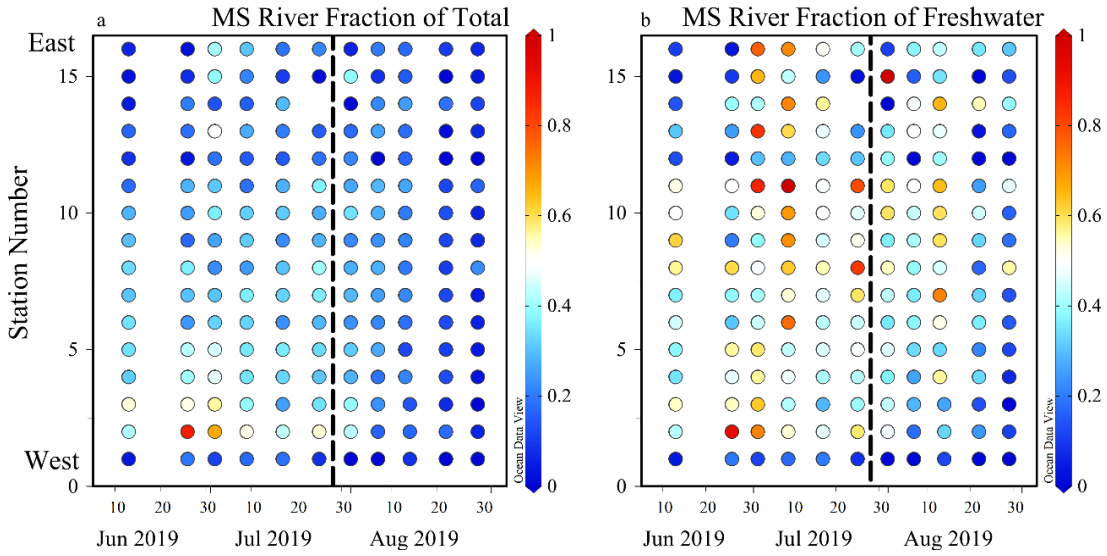


*Figure 3.4. Fraction of Mississippi River water of total surface water and the freshwater component of the surface water at each Bonnet Carré Spillway station*

Surface water data collected from BCS stations for (a) calculated fraction of Mississippi (MS) River water (out of MS River water, local river water, and seawater) and (b) calculated fraction of MS River water out of the freshwater present in the surface waters at each station. The vertical, black, dashed line indicates when the BCS closed on July 27. Station number generally increases with increasing distance from Lake Pontchartrain. Station 1 was primarily dominated by Pearl River outflow.

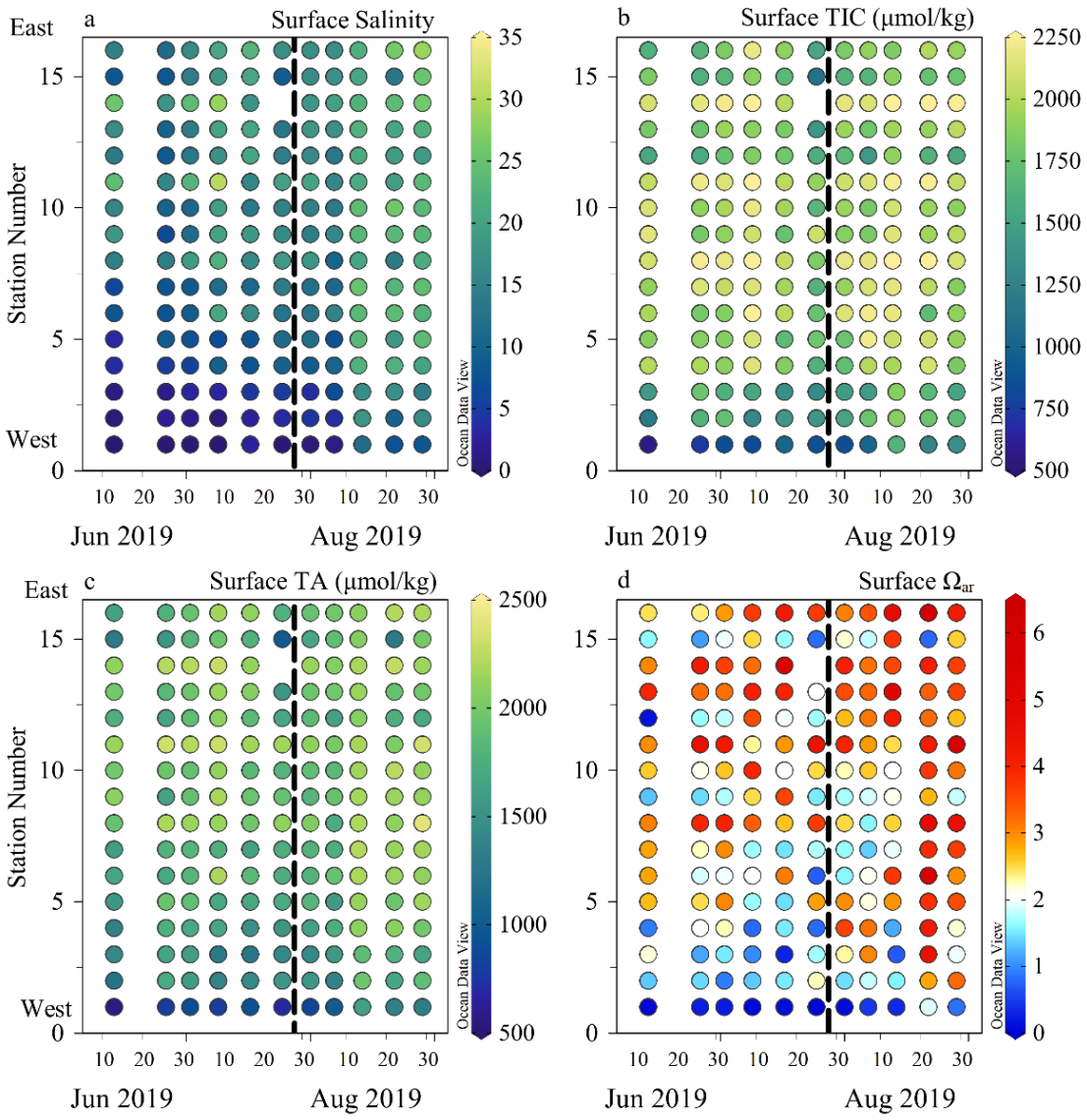


*Figure 3.5. Bonnet Carré Spillway sampling surface water salinty, TIC, TA, and $\Omega_{ar}$*

Surface water data collected from BCS stations for (a) salinity, (b) total inorganic carbon (TIC) (µmol/kg), (c) total alkalinity (TA) (µmol/kg), and (d) saturation state ($\Omega_{ar}$). Black dashed lines indicate the closure of BCS on July 27. Station number generally increases with increasing distance from Lake Pontchartrain.

### 3.4 Bonnet Carré Spillway Subsurface Data

Subsurface samples were collected at roughly 0.5 m from the bottom at each station. Bottom depths ranged from 1.5 m at coastal stations to 11 m at station 14 outside the barrier islands, with a majority of stations having a subsurface sampling depth between 2 to 6 m (Fig. 3.6). In subsurface waters, salinities were lowest (> 5) in the western-most stations of the Sound and at coastal stations (9, 12, and 15); most stations remained fairly saline (> 15) throughout the time-series (Fig. 3.7a). There was strong stratification between fresher surface waters and saltier subsurface waters until approximately 3 weeks after the BCS closed in the western Sound (Fig. 3.5a; Fig. 3.7a; Fig. 3.8; Fig. 3.10). TA was generally >2000 μmol/kg, except for BCS station 1 (near the Pearl River discharge) and at station 15 before the BCS closed, which was likely due to discharge from the Mobile River (Fig. 3.7c; Fig. 3.4b). TIC followed this same trend with most stations > 2000 μmol/kg throughout the study period (Fig. 3.7b). However, $\Omega_{ar}$ remained low (generally < 2) in subsurface waters throughout the Sound while the BCS was open and did not increase for the majority of stations until a month after the spillway had closed (Fig. 3.7f; Fig. 3.8; Fig. 3.10; Fig. 3.11). This was likely due to hypoxic conditions and elevated $pCO_2$ concentrations observed in subsurface waters throughout the Sound that persisted during the summer (Fig. 3.7d & e; Fig. 3.8; Fig. 3.9; Fig. 3.10; Fig. 3.11).

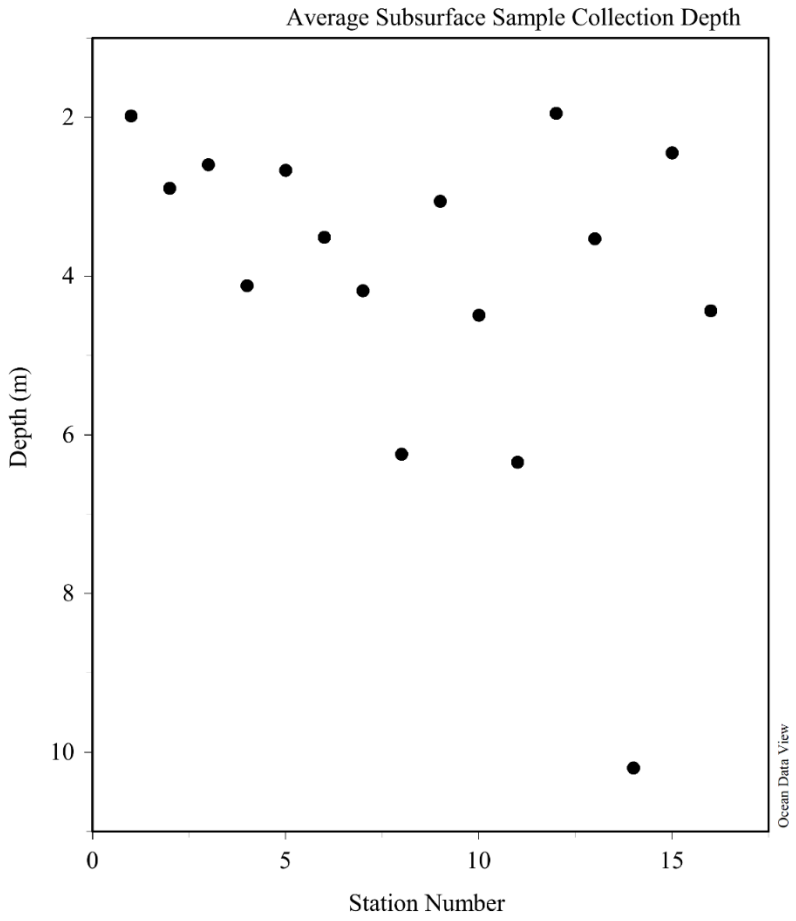


*Figure 3.6. Average depth that subsurface samples were collected for the BCS stations.*

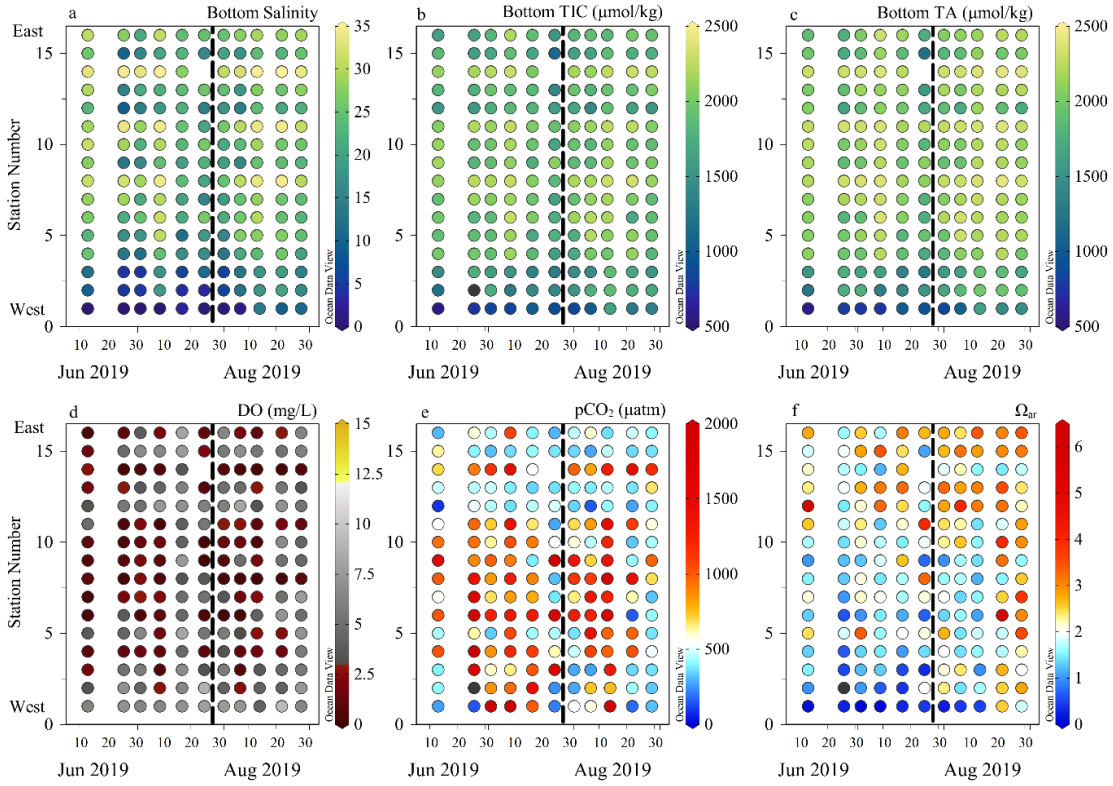


*Figure 3.7. Subsurface water data collected from BCS study for salinity, TIC, TA, DO, pCO2, and* $\Omega_{ar}$

Subsurface water data collected from BCS study for (a) salinity, (b) total inorganic carbon (TIC) (µmol/kg), (c) total alkalinity (TA) (µmol/kg) and (d) dissolved oxygen (mg/L), (e) $pCO_2$ (µatm), and (f) aragonite saturation ($\Omega_{ar}$). Black dashed lines indicate the closure of BCS on July 27. Station number generally increases with increasing distance from Lake Pontchartrain.

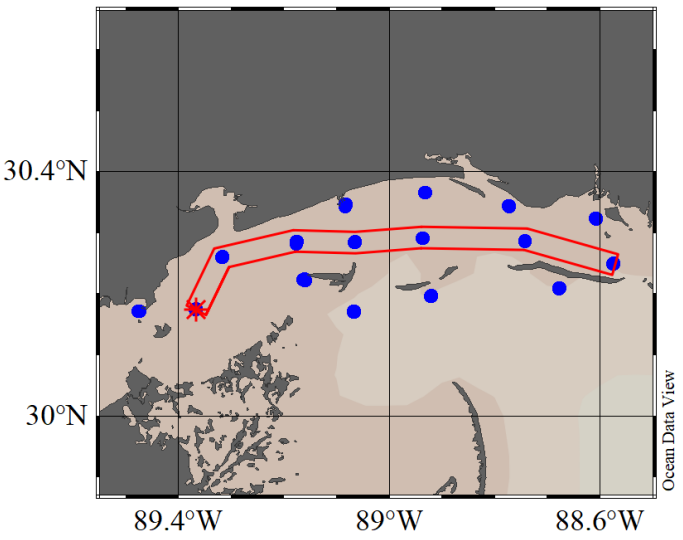
30.4°N
30°N
89.4°W
89°W
88.6°W
Ocean Data View

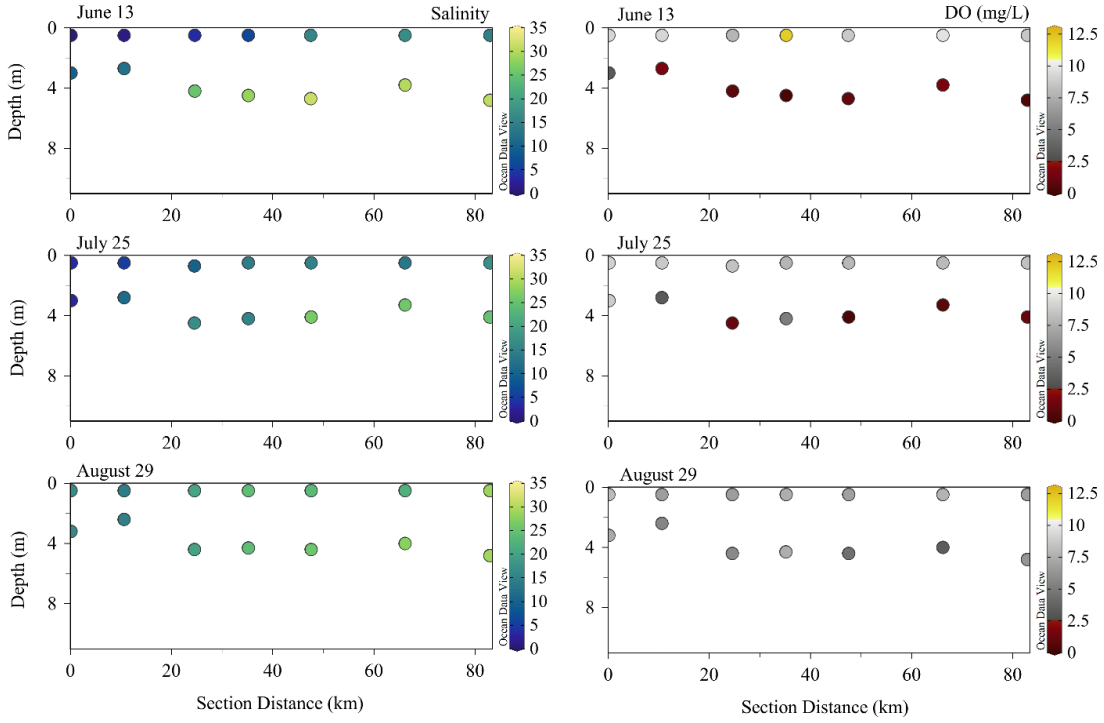
June 13
Salinity
July 25
August 29
Depth (m)
Section Distance (km)
Ocean Data View
June 13
DO (mg/L)
July 25
August 29
Section Distance (km)

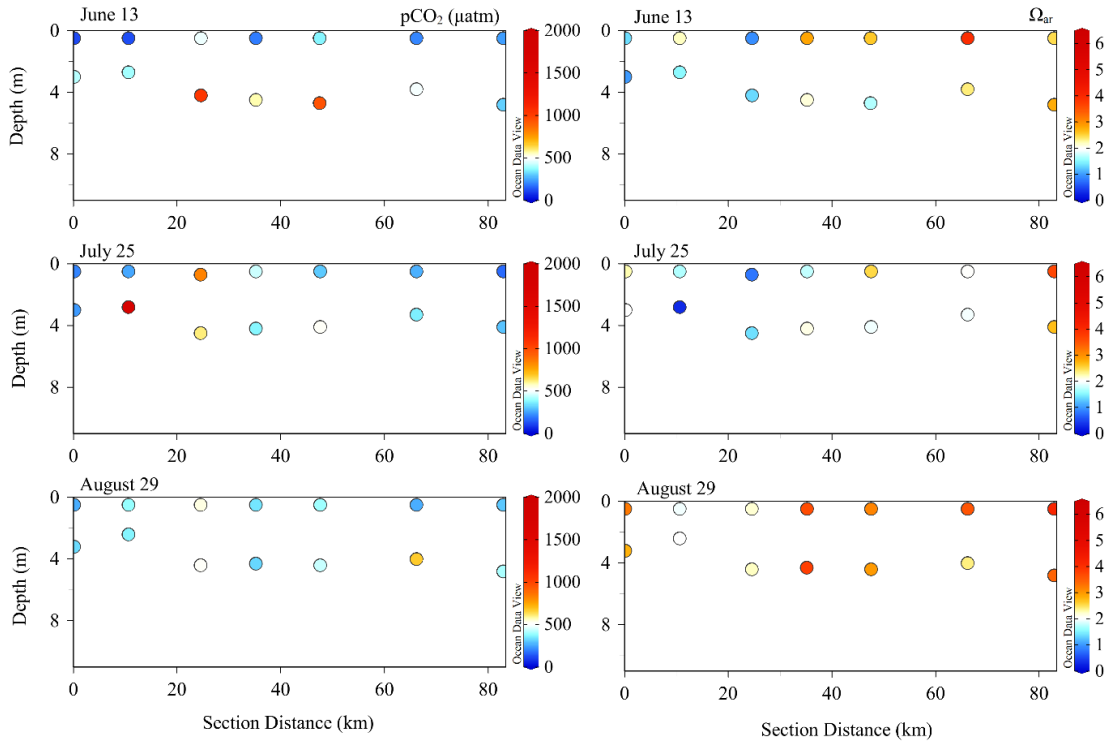


*Figure 3.8. Horizontal transect through the middle Sound, including salinity, DO, pCO2, and $\Omega_{ar}$ for surface and subsurface samples*

Horizontal transect through the middle Sound, including BCS stations 2, 3, 4, 7, 10, 13, and 16. Red star indicates where the transect begins (section distance = 0). Salinity (top left panels), dissolved oxygen (mg/L; top right panels), $pCO_2$ (µatm; bottom left panels), and aragonite saturation ($\Omega_{ar}$; bottom right panels) for surface and subsurface samples as a function of distance along the section are shown for the sampling dates June 13, July 25, and August 29.

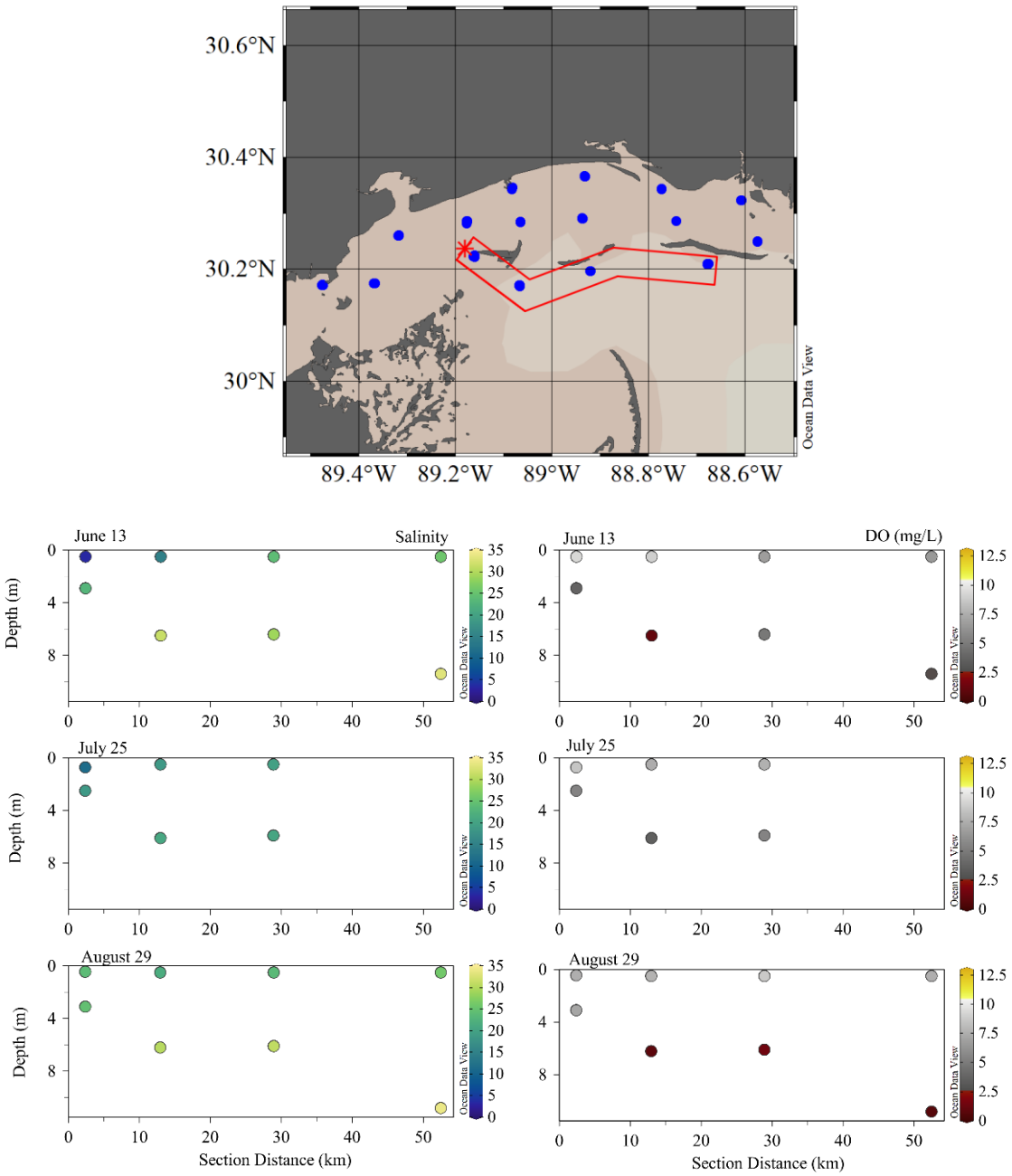
30.6°N
30.4°N
30.2°N
30°N
89.4°W
89.2°W
89°W
88.8°W
88.6°W
Ocean Data View
June 13
Salinity
July 25
August 29
Depth (m)
Section Distance (km)
DO (mg/L)

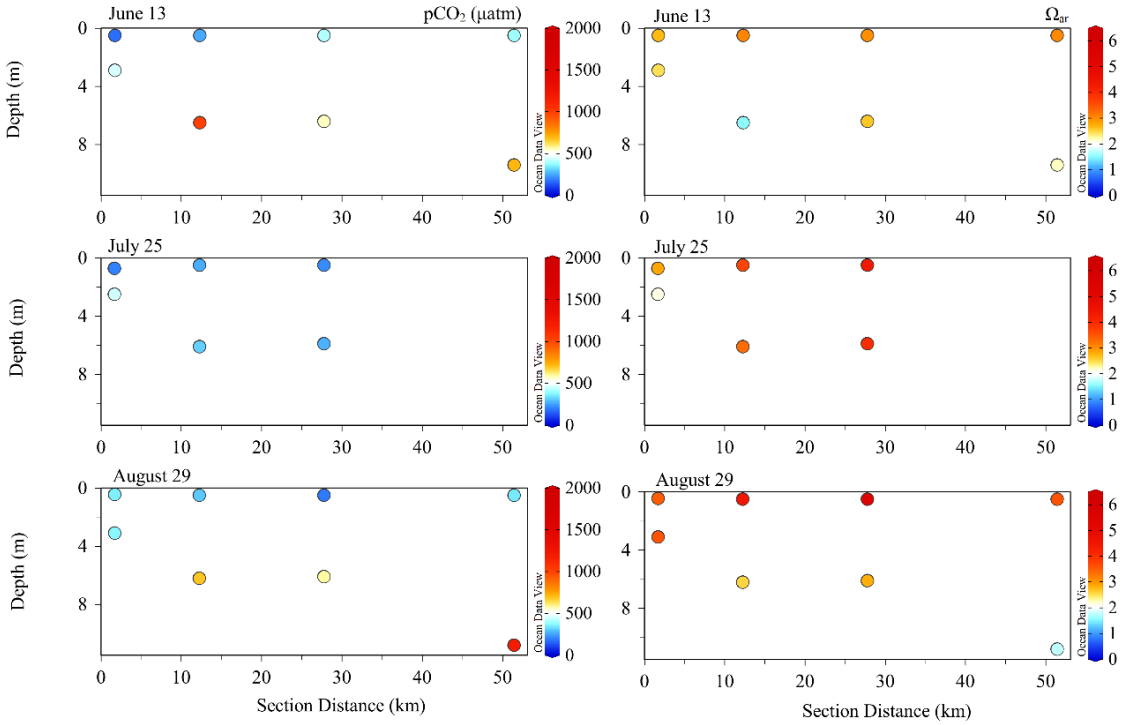


*Figure 3.9. Horizontal transect outside the Sound, including salinity, DO, pCO2, and $\Omega_{ar}$ for surface and subsurface samples*

Horizontal transect outside the barrier islands, including BCS stations 5, 8, 11, and 14. Red star indicates where the transect begins (section distance = 0). Salinity (top left panels), dissolved oxygen (mg/L; top right panels), $pCO_2$ (µatm; bottom left panels), and aragonite saturation ($\Omega_{ar}$; bottom right panels) for surface and subsurface samples as a function of distance along the section are shown for the sampling dates June 13, July 25, and August 29. Station 14 was not sampled on July 25 due to inclement weather.

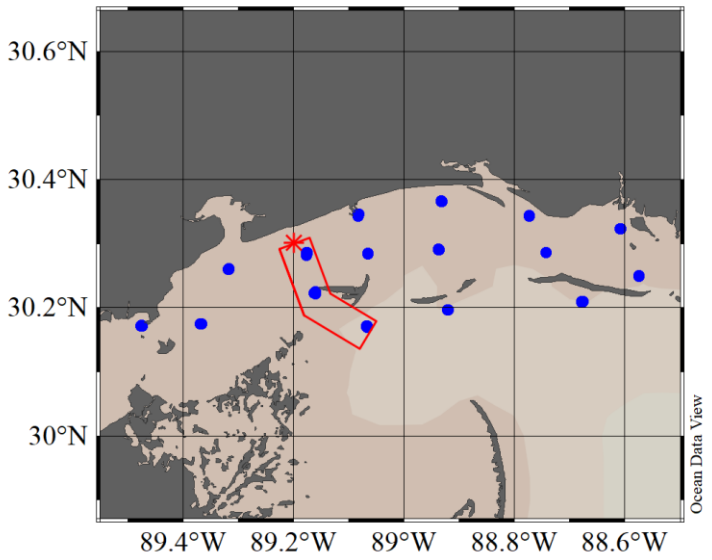
30.6°N
30.4°N
30.2°N
30°N
89.4°W
89.2°W
89°W
88.8°W
88.6°W
Ocean Data View

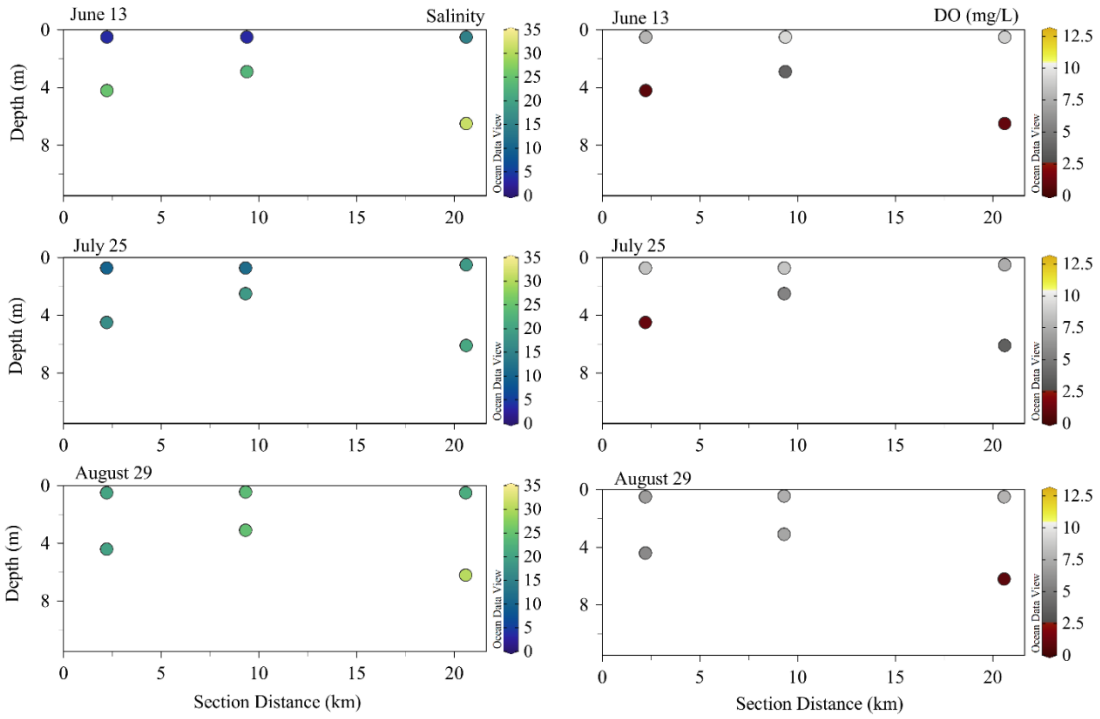
June 13
Salinity
July 25
August 29
Depth (m)
Section Distance (km)
Ocean Data View
June 13
DO (mg/L)
July 25
August 29
Depth (m)
Section Distance (km)
Ocean Data View

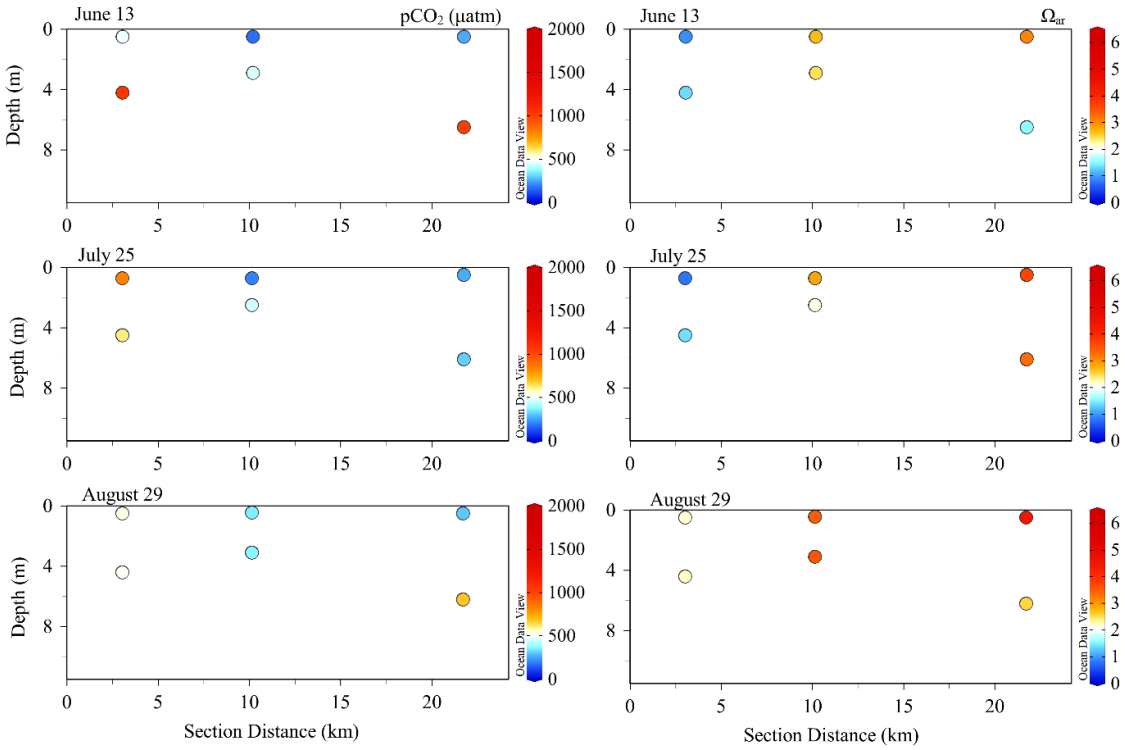


*Figure 3.10. Vertical transect for the western Sound, including salinity, DO, pCO2, and $\Omega_{ar}$ for surface and subsurface samples*

Vertical transect through the western Sound, including BCS stations 4, 5, and 8. Red star indicates where the transect begins (section distance = 0). Salinity (top left panels), dissolved oxygen (mg/L; top right panels), $pCO_2$ (µatm; bottom left panels), and aragonite saturation ($\Omega_{ar}$; bottom right panels) for surface and subsurface samples as a function of distance along the section are shown for the sampling dates June 13, July 25, and August 29.

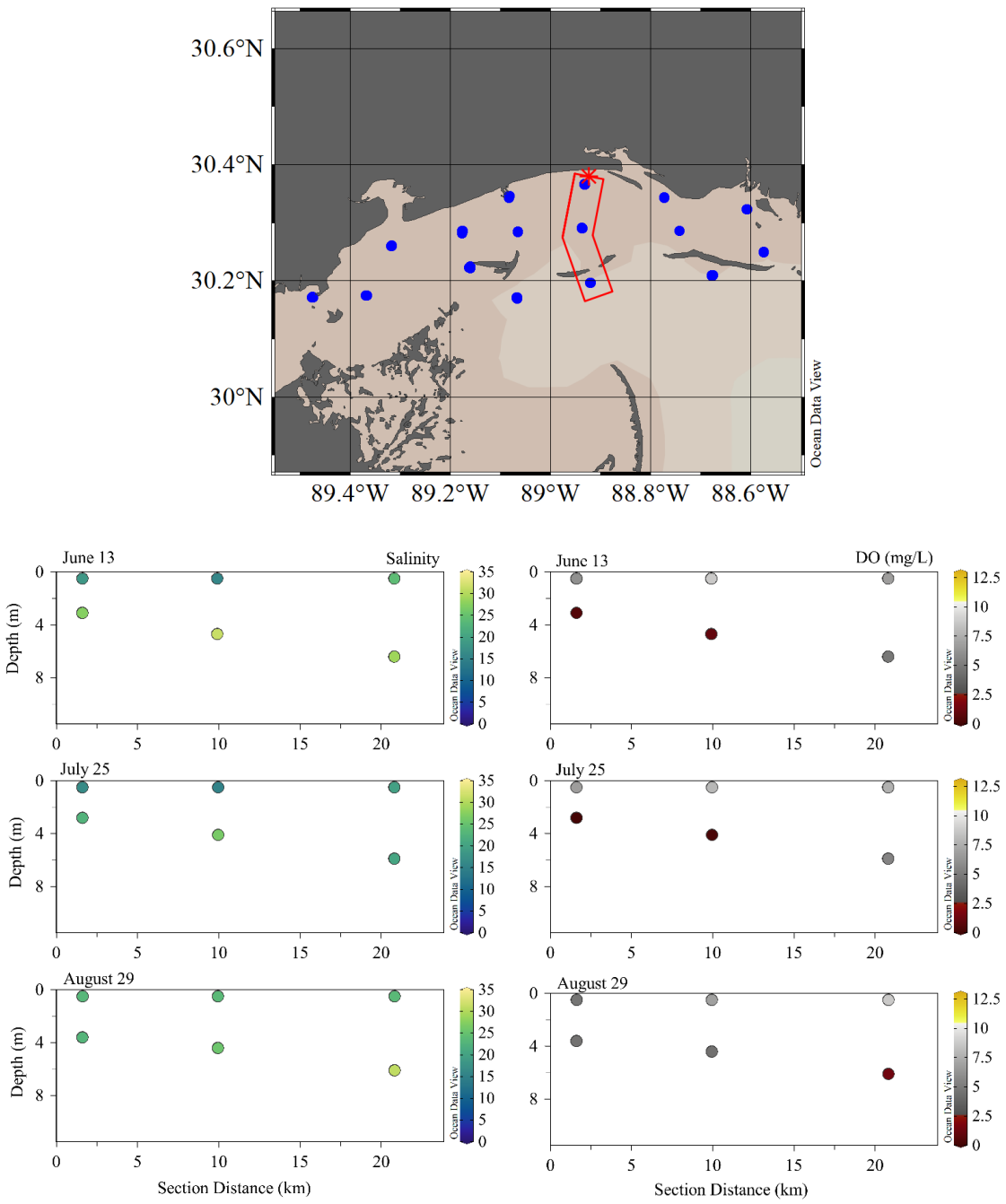
30.6°N
30.4°N
30.2°N
30°N
89.4°W
89.2°W
89°W
88.8°W
88.6°W
Ocean Data View
June 13
Salinity
July 25
August 29
Depth (m)
Section Distance (km)
DO (mg/L)

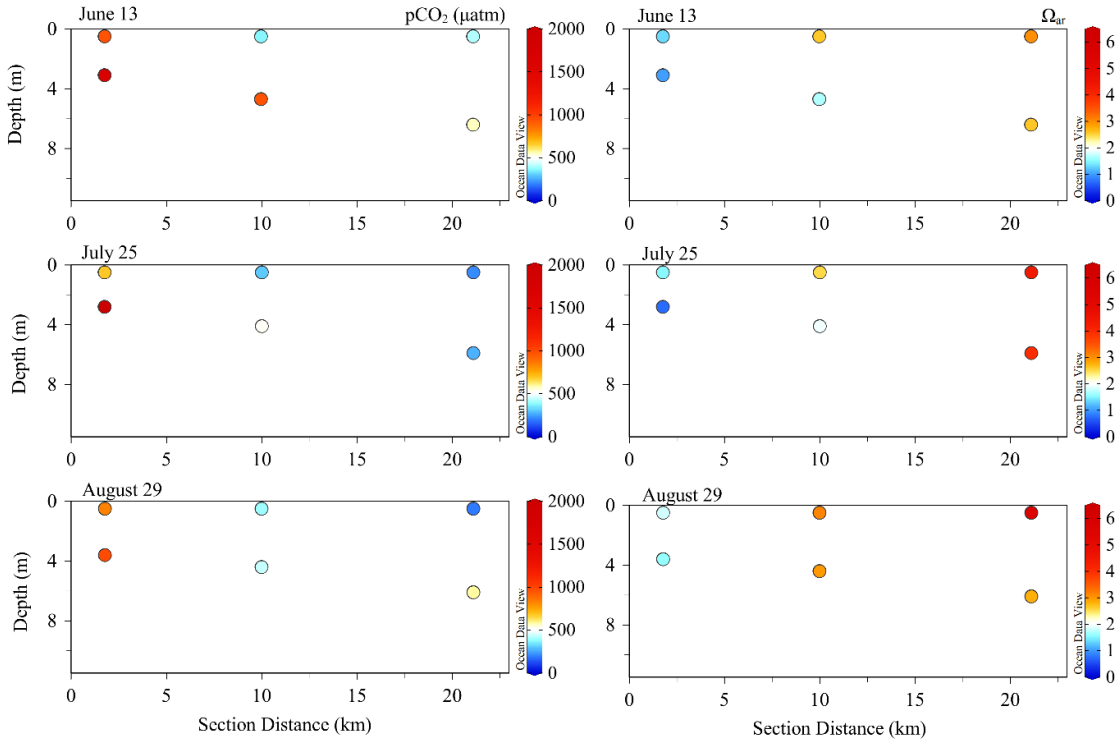


*Figure 3.11. Vertical transect for the middle Sound, including salinity, DO, pCO2, and $\Omega_{ar}$ for surface and subsurface samples*

Vertical transect through the middle Sound, including BCS stations 9, 10, and 11. Red star indicates where the transect begins (section distance = 0). Salinity (top left panels), dissolved oxygen (mg/L; top right panels), $pCO_2$ (µatm; bottom left panels), and aragonite saturation ($\Omega_{ar}$; bottom right panels) for surface and subsurface samples as a function of distance along the section are shown for the sampling dates June 13, July 25, and August 29.

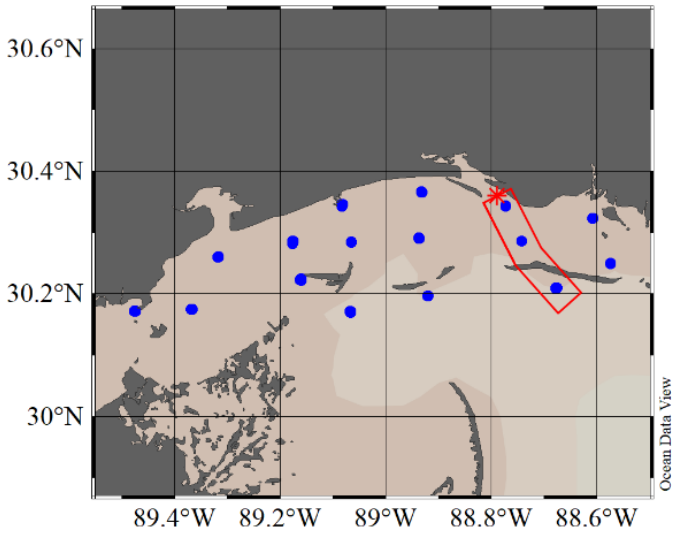
30.6°N
30.4°N
30.2°N
30°N
89.4°W
89.2°W
89°W
88.8°W
88.6°W
Ocean Data View

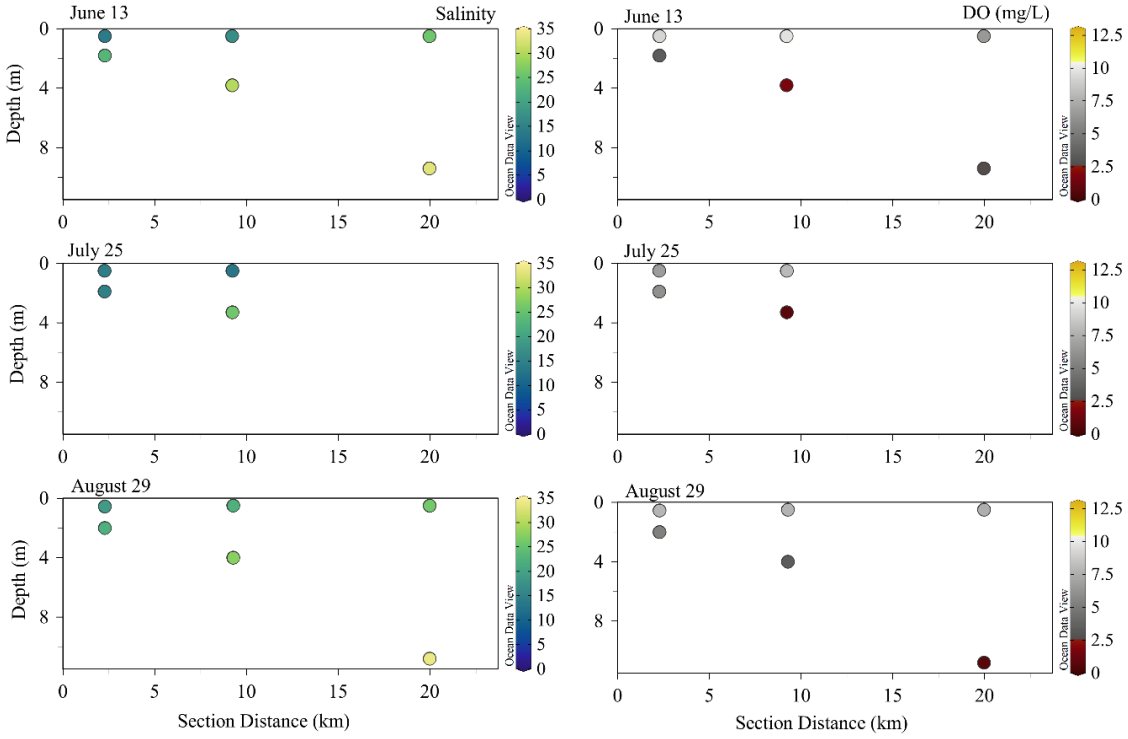
June 13
Salinity
July 25
August 29
Depth (m)
Section Distance (km)
Ocean Data View
June 13
DO (mg/L)
July 25
August 29
Section Distance (km)
Ocean Data View

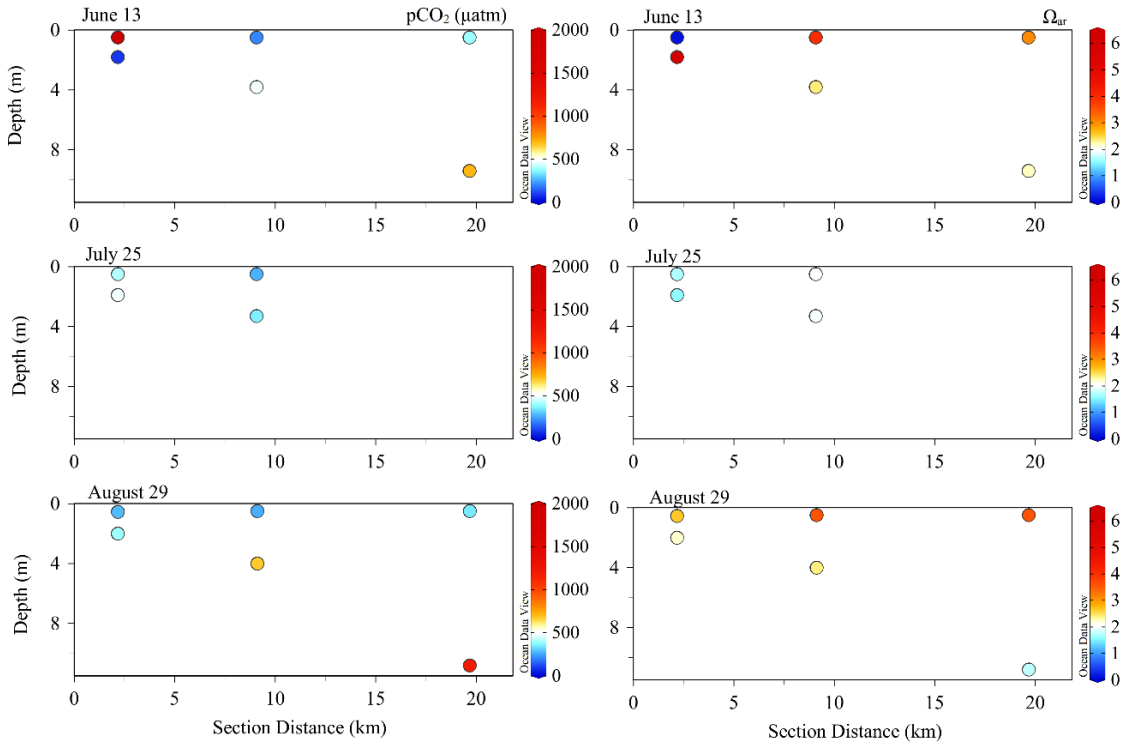


*Figure 3.12. Vertical transect for the eastern Sound, including salinity, DO, pCO2, and $\Omega_{ar}$ for surface and subsurface samples*

Vertical transect through the eastern Sound, including BCS stations 12, 13, and 14. Red star indicates where the transect begins (section distance = 0). Salinity (top left panels), dissolved oxygen (mg/L; top right panels), $pCO_2$ (µatm; bottom left panels), and aragonite saturation ($\Omega_{ar}$; bottom right panels) for surface and subsurface samples as a function of distance along the section are shown for the sampling dates June 13, July 25, and August 29. Station 14 was not sampled on July 25 due to inclement weather.

# CHAPTER IV – TEMPORAL CARBONATE TRENDS IN THE MISSISSIPPI SOUND

## 4.1 Beach Sampling Effective Freshwater Endmembers

We performed similar statistical analyses on the beach dataset as for the Bonnet Carré. In the BCH data, TA showed a positive correlation with salinity ($r$ = 0.85, df = 62, $p < 0.01$) with greatest variability at low salinities (Fig. 4.1a). This correlation indicates that TA distribution is mostly conservative for our study region (Fig. 4.1a). TIC had similar trends with salinity as TA but had a lower correlation coefficient ($r$ = 0.77, df = 62, $p < 0.01$) and, thus, generally behaved less conservatively in this area (Fig. 4.1b). Using BCH samples, we determined that the effective freshwater TA endmember (derived from the y-intercept of the linear regression between TA and salinity) for this region was 731 ± 64 μmol/kg and an effective freshwater TIC endmember of 778 ± 70 μmol/kg) (Fig. 4.1a & b). This effective endmember falls between the measured values for the Mobile and Pearl Rivers at 862 and 530 μmol/kg (TIC= 844 and 567 μmol/kg), respectively (Fig.4.1 a & b; Table 3.1). All other rivers in the area had measured TA values < 400 μmol/kg and TIC <450 μmol/kg (Table 3.1). While the simple (Model I) linear regression was used assuming salinity is an independent variable, similar conclusions are reached about the apparent freshwater endmembers using a Model II type linear regression which assumes both salinity and TA are dependent variables (e.g., 607 ± 66 μmol/kg for effective TA endmember using Model II regression).

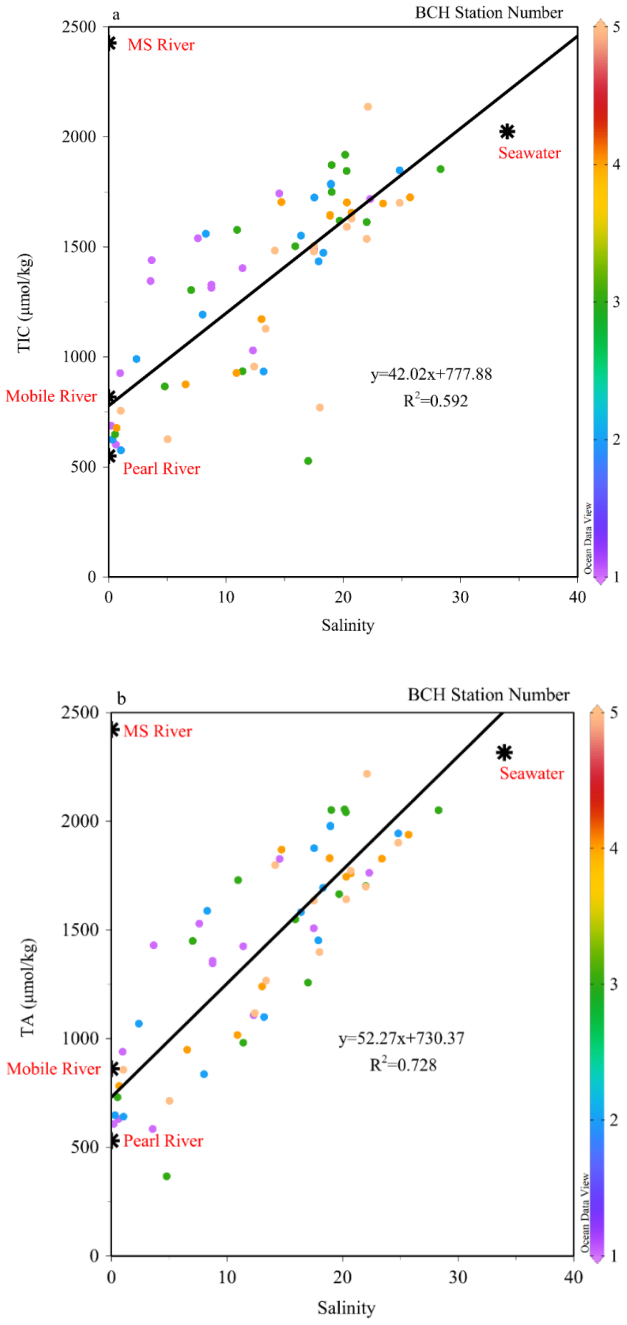


*Figure 4.1. Beach sample effective (a) TIC and (b) TA endmembers*

(a) Total inorganic carbon (TIC) (μmol/kg) and (b) total alkalinity (TA) (μmol/kg) from monthly BCH samples vs. salinity. Black stars indicate measured endmembers (labeled with individual rivers) and were not included in the linear regression and statistical calculations.

### 4.2 Temporal Trends of Coastal Stations

Data from the beach sampling were compared with adjacent coastal BCS stations due to the lack of monthly beach sampling during June and July 2019, which resulted from the resources required to conduct the BCS sampling on a weekly basis during the summer. Comparing the monthly beach sampling data with the three coastal stations from the BCS sampling adjacent to the BCH sampling sites in the western Sound (3, 6, & 9), there was a general decrease in TA and TIC from late summer/fall into the winter/early spring months with a minimum in late March at an average of ~829 μmol/kg. (Fig. 4.2b & c). BCS station 1 was excluded in this analysis due to the direct influence of the Pearl River observed at the station throughout summer (Fig. 3.4b). There was a strong increase in TA and TIC after the second opening of the BCS observed between late May and August (Fig. 4.2 & c). This pattern was observed in the salinity and $\Omega_{ar}$ data as well (Fig. 4.2a & d). The lowest average salinity was observed during the second opening of the spillway and the salinity did not return to values similar to those observed pre-spillway opening until about a month after the BCS closed (Fig. 4.2a). The average $\Omega_{ar}$ nearly doubled in surface waters while the BCS was open (Fig. 4.2d). TIC, TA, and $\Omega_{ar}$ reached the highest values observed approximately one month after the BCS closed; they returned to values similar to those observed in the year prior approximately 3 months after the BCS closed (Fig. 4.2).

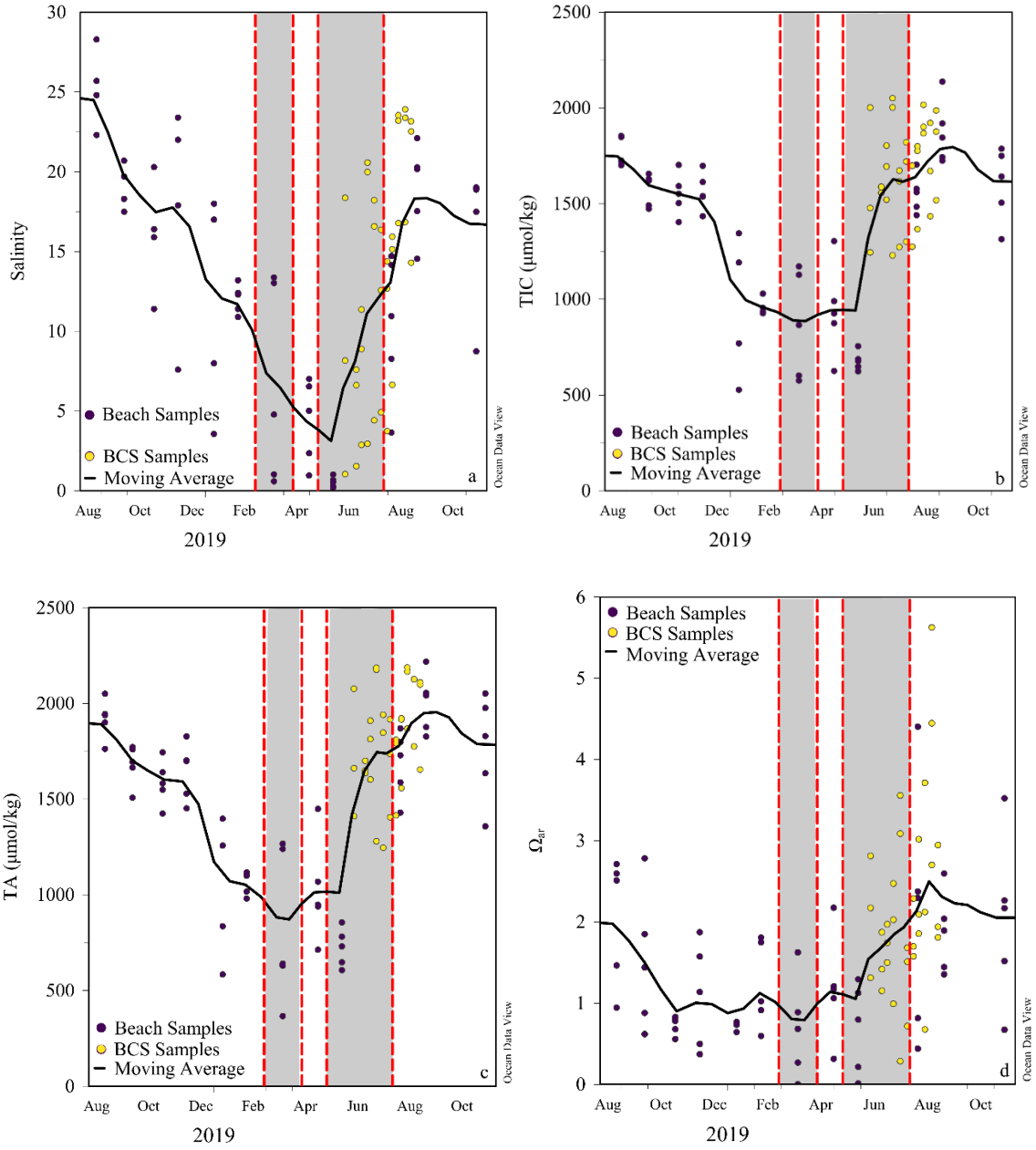


*Figure 4.2. Temporal salinity, TIC, TA, and $\Omega_{ar}$ trends*

(a) Salinity, (b) total inorganic carbon (TIC) (µmol/kg), (c) total alkalinity (TA) (µmol/kg) and (d) aragonite saturation ($\Omega_{ar}$) measured from monthly beach samples (purple circles) and coastal BCS stations 3, 6, and 9 (yellow circles) from August 2018 to

November 2019. Black lines indicated the moving monthly average throughout the year. The gray shaded areas bordered by red dashed lines indicate when the BCS was open.

### 4.3 $pCO_2$ Flux Data

During the study, the Mississippi coast generally acted as a source of $CO_2$ to the atmosphere, with positive flux values indicating a flux into the atmosphere while negative values indicate when the Sound acted as a sink for atmospheric $CO_2$ (Fig. 4.3). The majority of the calculated fluxes at each station generally fall above the red equilibrium line, with the exception of winter months and following periods of increased river discharge. However, given the error associated with the $pCO_{2(water)}$ measurements, it is difficult to assess whether the Sound is acting as a source or sink based on these 5 beach sites and their variabilities being much larger than the calculated fluxes. Therefore, having a larger data set, like during the BCS sampling, or a direct $pCO_2$ sensor like that at the Coastal LA PMEL buoy would more accurately answer whether this region acts as a source or sink for $CO_2$. We did observe that the largest decreases in $pCO_2$ usually occurred following increased discharge from either the Pearl or Mobile Rivers, as observed between August to September 2018, November to December 2018, and January to February 2019 (Fig. 4.3). The observed decrease in $CO_2$ flux during the summer 2019 was likely due to the flux of freshwater from the Mississippi River through the BCS and not from the local rivers that had relatively low discharge during this time period (Fig 4.3). This demonstrated influence of the local rivers on $CO_2$ flux, which supports our previous notion that the decreases in $CO_2$ flux in summer 2019 are driven by increased freshwater flux from the Mississippi River. This idea could be followed up with more

intensive sampling as mentioned previously to reduce the error and variability in the data. The spatial variability between the calculated fluxes indicates that a larger sampling set or more accurate direct measure of $pCO_{2(water)}$ (like those from the Coastal LA PMEL buoy) would allow to more accurately assess whether the Sound as a whole acts as a source or sink for $CO_2$.

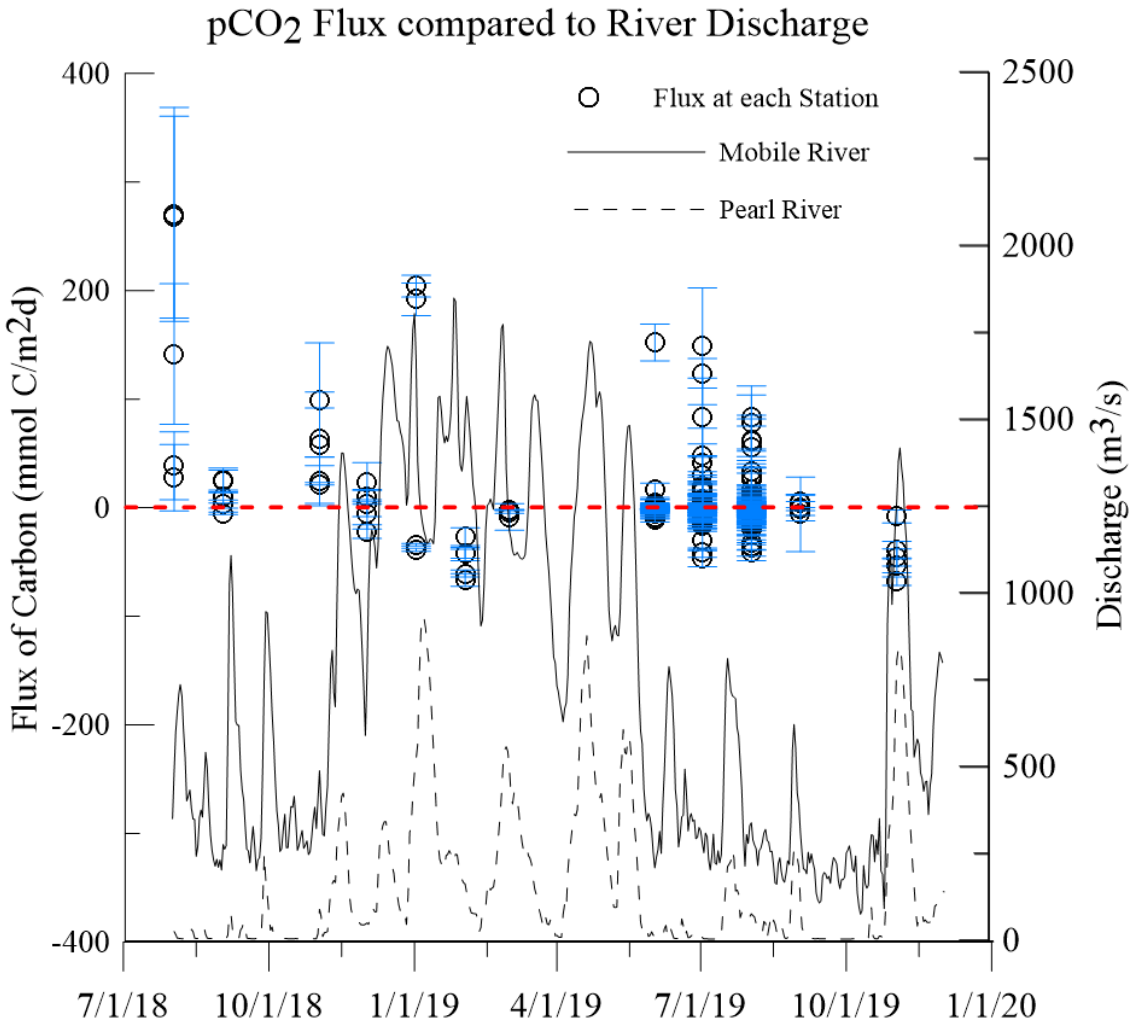


*Figure 4.3. Monthly carbon flux compared to river discharge data*

Calculated $pCO_2$ fluxes for all stations (white circles) throughout the study period. Daily-averaged discharge data accessed from USGS for the Pearl River (dashed line) and Mobile River (solid line) are plotted in $m^3/s$. The red dashed line is equal to no net flux of $CO_2$, where points above that line indicate a source of $CO_2$ and below the line are a sink. Absolute error from propagation calculations for each flux is shown with the blue bars. One sample point in March was excluded as an outlier due to error >400%.

# CHAPTER V – DISCUSSION

The TA values measured in the Mississippi Sound during this study were generally lower than those observed in previous studies offshore of estuaries within the northern Gulf of Mexico. TA generally ranges from 2325 to 2400 µmol/kg at salinities from 24 to 25 along the coast of the northern Gulf of Mexico (Wang et al. 2013), though samples from flow-through systems and surface bottles from the GOMECC-3 cruise in July-August 2017 showed TA values as low as 2050 µmol/kg, with salinity as low as 24, near the shelf-break across the Mississippi Bight (Barbero et al. 2019). Our study observed a range in TA values for beach samples from 584 µmol/kg to 2210 µmol/kg, with an average of 1447 µmol/kg for the beach sampling data (Fig. 4.1a). The beach sites experienced a wide range of salinities, with values near 1 at BCH station 1 while the BCS was open, and up to 28 in late summer (Fig. 4.2a). The lower observed TA in this region from winter to early summer is likely due to the increased input of low alkalinity freshwater from local Mississippi and Alabama rivers, like the Pearl River, into the system (Fig. 4.2c; Fig. 4.3; Table 3.1). These less alkaline rivers may leave the system more vulnerable to increased inputs of $CO_2$ into the ocean from anthropogenic emissions. The reduced alkalinity of the system will result in decreased buffering capacity and decreased saturation states, which will likely be harmful to local oyster reefs.

Notably, while the BCS was open, the range in TA was elevated, with upper values similar to those previously observed in the northern Gulf of Mexico and coastal Texas area with a range from 559 µmol/kg (845 µmol/kg excluding station 1 which is heavily influenced by the low-alkalinity Pearl River) to 2410 µmol/kg (2242 µmol/kg excluding stations outside the barrier islands), with an average of 1896 µmol/kg. The

range in salinity for the BCS samples was from a minimum of 0.14 in the western Sound stations to a maximum of 35 at the stations outside the barrier islands (31 for stations inside the Sound) (Fig. 3.1; Fig. 3.5; Fig. 3.7). The observed increase in the effective TA endmember is likely due to the increased flux of higher alkalinity Mississippi River water into the Sound (Fig. 3.4). During this time, there was also reduced discharge from the Pearl and Mobile Rivers, resulting in a decreased source of low alkalinity water to the Sound (Fig. 4.3). High TA while the BCS was open is likely the reason for the observed increase in saturation state during the summer at the coastal stations, which were experiencing decreased saturation states during winter and spring (Fig. 4.2d). However, the large flux of freshwater during this time from the BCS likely still made conditions unfavorable for local oysters (Fig. 4.2a).

In addition, the TIC values observed in this study were similar to DIC values found in Mississippi plume waters with surface values near 1860 µmol/kg and subsurface (~25-400 m) values from 2000-2200 µmol/kg (Wang et al. 2013). The BCH samples had a range in DIC from 530 to 1860 µmol/kg (Fig. 4.1a) and the BCS samples had a range in TIC from 600 (930 µmol/kg without BCS station 1) to 2300 µmol/kg (Fig. 3.1a). Therefore, the relative increase in TA compared to TIC may have resulted in an increase TA/TIC ratio, which also resulted in the observed increase in saturation state. TIC generally behaved less conservatively than TA (Fig. 3.2a), which is likely due to biological consumption that resulted in lower measured values than those predicted by the endmember model. In comparison, generally biological removal of TA is relatively low compared to the total concentrations in seawater. The relative conservative behavior

of TA and more non-conservative behavior of TIC supports findings from nearby coastal carbon cruises in the northern Gulf of Mexico (Wang et al. 2013).

The low saturation states observed during our study indicate that this area may be susceptible to future ocean acidification. Average values for the saturation states during this study were always below 2.5, with averages < 1 from late fall to early summer (Fig. 4.2d). In comparison, nearby studies have found supersaturated aragonite saturation conditions in shelf and upper slope waters the northern Gulf of Mexico typically ranging from 2.5 to 4.0, with inner Louisiana shelf waters impacted by the Mississippi River as high as 5.0 (Wang et al. 2013). The period of observed undersaturated conditions in Mississippi Sound (late fall to early summer; Fig. 4.2d) is also significant since this is when newly spawned juvenile oysters are attempting to mature into sexually mature adults (Hayes and Menzel 1981; Shumway 1996). Reduced saturation states within the Mississippi Sound during this crucial developmental period for the juvenile oysters may have contributed to the reduction in oyster landings over recent years (Posadas 2019).

While the BCS was open, there was an observed increase in average saturation state in surface water at the coastal stations (Fig. 4.2d). However, $\Omega_{ar}$ values were lowest in surface and subsurface stations primarily in the western Sound and at coastal stations in comparison with other station in the Sound (Fig. 3.5d; Fig. 3.7f; Fig. 3.8). This is likely due to the fact that the Mississippi River is primarily a bicarbonate dominated system (Cai 2003), whereas the saturation state is determined by carbonate and calcium ion concentrations (Kleypas et al. 1999). Therefore, despite the overall increase in TA, there was a minimal effect on surface saturation states (Fig. 4.2c & d). Subsurface waters also were undersaturated while the BCS was open, likely due to both increased

stratification and increased respiration in the bottom waters (Fig. 3.7; Fig. 3.8). Increased respiration in subsurface waters would increase in situ $CO_2$ through the breakdown of sinking organic material supplied from the surface primary productivity. The hypoxia and stratification in the Sound is likely also exacerbated by the decreased winds during the spring and early summer months in the Mississippi Sound (Parra et al. 2020). Saturation states at the westernmost Sound stations did not appear to increase to saturated conditions until approximately 3-4 weeks after the BCS had closed (Fig. 3.7). The increase in saturation state was due to decreased freshwater inputs and decreased hypoxia in subsurface waters throughout the Sound (Fig. 3.4; Fig. 3.7).

The Mississippi coast acted as a source for $CO_2$ throughout most of the study period, with the exception of February and November 2019 (Fig. 4.3). However, after times of peak discharge from the local Pearl and Mobile Rivers, there were substantial decreases in the $pCO_2$ fluxes out of the Sound (Fig. 4.3). This may have been due to increased nutrient delivery from the rivers that stimulated increased primary productivity, consuming excess $CO_2$ in the water column. The observed nutrient concentrations remained relatively low at coastal stations (BCH) throughout the study, with soluble reactive phosphate ranging from 0.1 to 8.1 µmol/kg (average = 1.1 ± 1.5 µmol/kg), which is consistent with consumption from primary producers. Reduced sea-to-air $CO_2$ fluxes were also found in the northern Gulf of Mexico during periods of increased discharge from the Mississippi-Atchafalaya River System and subsequent increases in dissolved inorganic nitrogen loads (Xue et al. 2016; Lohrenz et al. 2018). However, these prior studies showed that the shelf waters served as a net sink for $pCO_2$ in winter and spring (Xue et al. 2016; Lohrenz et al. 2018); our study indicated coastal areas likely served as

sources for $pCO_2$ for most of the year. Furthermore, while the BCS was open, the $pCO_2$ flux decreased, showing that the Sound acts as less of a source for $CO_2$ and was transitioning to sink conditions in summer due to the enhanced primary production from increased nutrient flux from the Mississippi River (Fig. 4.3). Therefore, the flux of $CO_2$ in these coastal areas may vary not only seasonally but also in response to the magnitude and source of freshwater to the region.

# CHAPTER VI – CONCLUSIONS

The contribution of the less alkaline, local rivers in Mississippi and Alabama may leave the Mississippi Sound more susceptible to ocean acidification in fall and winter months. Low TA and $\Omega_{ar}$ observations are relevant because they co-occur with the vulnerable period of juvenile oyster maturation. During this study, both TA and $\Omega_{ar}$ increased during the summer and early fall months; this was likely due to the large influence of the Bonnet Carré Spillway, which delivered high alkalinity Mississippi River water to the Sound between February and July 2019. Despite the average increase in surface TA and $\Omega_{ar}$ values, bottom water $\Omega_{ar}$ remained < 2 throughout the summer. This was primarily due to hypoxic and elevated $pCO_2$ conditions driven by freshwater stratification and increased primary productivity in surface waters that enhanced subsurface respiration. Substantial seasonal inputs of Mississippi River water from the Bonnet Carré Spillway could represent a new normal in the Sound's hydrography during spring and summer months, since it has been opened more in the past decade than any previous decade since it was constructed (https://www.mvn.usace.army.mil/Missions/Mississippi-River-Flood-Control/Bonnet-Carre-Spillway-Overview/Historic-Operation-of-Bonnet-Carre/ accessed 05/16/2020). Seasonal fluctuations of TA and $\Omega_{ar}$ with generally low aragonite saturation states indicate the system is not well buffered to environmental change. Low aragonite saturation will be detrimental to oyster stocks in the Mississippi Sound; thus, it is imperative that we understand the carbon system and the regional environmental stressors that influence the Mississippi Sound ecosystem.

Future work in this region could be aimed towards establishing a more permanent time-series data monitoring station near the oyster reefs in the western Sound and in Mobile Bay, similar to the PMEL Coastal La buoy, to measure $CO_2$ and pH throughout the year. Additionally, previous research has suggested that this region can be influenced by inputs of submarine groundwater (Sanial et al. 2019). Submarine groundwater could contribute increased nutrients (Rodellas et al. 2015) and low oxygen water (Peterson et al. 2016) to the subsurface waters in the region, both of which could affect local carbonate chemistry. This region could benefit from continued monitoring, as this study was not able to provide summer data without the impacts of this extreme Bonnet Carré Spillway event. In addition, this system is under increasing pressure from increased freshwater inputs, eutrophication, hypoxia, harmful algal blooms and ocean acidification. There is lack of knowledge in how these multiple stressors affect one another and influence ocean acidification in coastal ecosystems. Therefore, since the Mississippi Sound is impacted by many of these stressors, further research in this region could contribute to predictions of coastal acidification stressors worldwide.

# REFERENCES


Barbero, L., and others. (2019). Third Gulf of Mexico Ecosystems and Carbon Cycle (GOMECC-3) Cruise. NOAA Cruise Report doi 10.25923/y6m9-fy08. Retrieved from https://repository.library.noaa.gov/view/noaa/21256 on April 26, 2020.

Bianchi, T. S., J. R. Pennock, R. R. Twilley. 1999. Biogeochemistry of Gulf of Mexico Estuaries. John Wiley & Sons.

Brunner, C. A., J. M. Beall, S. J. Bentley, and Y. Furukawa. 2006. Hypoxia hotspots in the Mississippi Bight. J. Foramin. Res. **36**: 95–107. https://doi.org/10.2113/36.2.95

Cai,W. J., Y, Wang, R. E. Hodson. 1998. Acid–base properties of dissolved organic matter in the estuarine waters of Georgia, USA. Geochim. Cosmochim. Acta **62**: 473–483.

Cai, W. J. 2003. Riverine inorganic carbon flux and rate of biological uptake in the Mississippi River plume. Geophys. Res. Lett. **30**: 1032. https://doi.org/10.1029/2002GL016312

Cai, W. J. and others. 2011. Acidification of subsurface coastal waters enhanced by eutrophication. Nature Geosci. **4**: 766–770.

Dickson, A. G. 1981. An exact definition of total alkalinity and a procedure for the estimation of alkalinity and total inorganic carbon from titration data. Deep Sea Res. **28**: 609–623.

Dickson, A. G. 1990. Standard potential of the reaction: $AgCl(s) + 12H_2(g) = Ag(s) + HCl(aq)$, and the standard acidity constant of the ion $HSO_4^-$ in synthetic sea water

from 273.15 to 318.15 K. J. Chem. Thermodyn. **22**: 113–127. https://doi.org/10.1016/0021-9614(90)90074-Z

Dickson, A.G., Sabine, C.L. and Christian, J.R. (Eds.) 2007. Guide to Best Practices for Ocean CO2 Measurements. PICES Special Publication 3, 191 pp.

Doney, S. C. 2010. The growing human footprint on coastal and open–ocean biogeochemistry. Science **328**: 1512–1516.

Dugas, R. J., E. A. Joyce, and M. E. Berrigan. 1997. History and status of the oyster, *Crassostrea virginica*, and other molluscan fisheries of the U.S. Gulf of Mexico, p. 187–210. *In* Mackenzie Jr., C. L., V. G. Burrell Jr., A. Rosenfield, and W. L. Hobart [eds.], The history, present condition, and future of the molluscan fisheries of North and Central America and Europe. Volume 1, Atlantic and Gulf Coasts. U.S. Dep. Commer., NOAA Tech. Rep. 127, 234 p.

Eleuterius, C. K. and S. L. Beaugez. 1979. Mississippi Sound: a hydrographic and climatic atlas. Mississippi–Alabama Sea Grant Consotium, Ocean Springs, Mississippi. MASGP–79–009.

Feely, R. A., R. R. Okazaki, W. J. Cai, N. Bednaršek, S. R. Alin, R. H. Byrne, and A. Fassbender. 2018. The combined effects of acidification and hypoxia on pH and aragonite saturation in the coastal waters of the California current ecosystem and the northern Gulf of Mexico. Cont. Shelf Res. **152**: 50–60.

Galtsoff, P. S. 1964. The American oyster, *Crassostrea virginica* (Gmelin). Fishery Bull. **64**: 1–480.

Gran, G. 1952. Determination of the equivalence point in potentiometric titrations. Part II. Analyst **77**: 661-671.

Hayes, P. F. and R. W. Menzel. 1981. The reproductive cycle of early setting *Crassostrea virginica* (Gmelin) in the Northern Gulf of Mexico, and its implications for population recruitment. Bio. Bull. **160**: 80–88.

Ho, P., M. J. Shim, S. D. Howden, and A. M. Shiller. 2019. Temporal and spatial distributions of nutrients and trace elements (Ba, Cs, Cr, Fe, Mn, Mo, U, V and Re) in Mississippi coastal waters: influence of hypoxia, submarine groundwater discharge, and episodic events. Cont. Shelf Res. **175**: 53–69. https://doi.org/10.1016/j.csr.2019.01.013

Hsu, S. A., E. A. Meindl, and D. B. Gilhousen. 1994. Determining the power–law wind–profile exponent under near–neutral stability conditions at sea. J. Appl. Meteorol. **33**: 757–765.

Kjerfve, B. 1983. Analysis and synthesis of oceanographic conditions in Mississippi Sound, April–October 1980. US Army Corps of Engineers.

Kleypas, J. A., R. W. Buddemeier, D. Archer, J. P. Gattuso, C. Langdon, and B. N. Opdyke. 1999. Geochemical consequences of increased atmospheric carbon dioxide on coral reefs. Science **284**: 118–120.

Laurent, A., K. Fennel, W. J. Cai, W. J. Huang, L. Barbero, and R. Wanninkhof. 2017. Eutrophication–induced acidification of coastal waters in the northern Gulf of Mexico: insights into origin and processes from a coupled physical–biogeochemical model. Geophys. Res. Lett. **44**. https://doi.org/10.1002/2016GL071881

Lee, D. D. 1990. The structure and mechanism of growth of calcium carbonate minerals in early stages of shells of the oyster *Crassostrea virginica*. J. Cryst. Growth **102**: 262–268.

Lee, K., T.-W. Kim, R. H. Byrne, F. J. Millero, R. A. Feely, and Y.-M. Liu. 2010. The universal ratio of boron to chlorinity for the North Pacific and North Atlantic oceans. Geochim. Cosmochim. Acta **74**: 1801–1811. https://doi.org/10.1016/j.gca.2009.12.027

Lemasson, A. J., S. Fletcher, J. M. Hall–Spencer, A. M. Knights. 2017. Linking the biological impacts of ocean acidification on oysters to changes in ecosystem services: a review. J. Exp. Mar. Biol. Ecol. **492**: 49–62.

Logan, C. A. 2010. A review of ocean acidification and America's response. BioScience. **60**: 819–828. https://doi.org/10.1525/bio.2010.60.10.8

Lohrenz, S. E. and W. J. Cai. 2006. Satellite ocean color assessment of air–sea fluxes of CO2 in a river-dominated coastal margin. Geophys. Res. Lett. 33: L01601, https://doi.org/10.1029/2005GL023942

Lohrenz, S. E., W.J. Cai, S. Chakraborty, W.J. Huang, X. Guo, R. He, Z. Xue, K. Fennel, S. Howden, and H. Tian. 2018. Satellite estimation of coastal pCO2 and air-sea flux of carbon dioxide in the northern Gulf of Mexico. Remote Sens. Environ. 207: 71–83.

Lueker, T. J., A. G. Dickson, and C. D. Keeling. 2000. Ocean $pCO_2$ calculated from dissolved inorganic carbon, alkalinity, and equations for $K_1$ and $K_2$: validation

based on laboratory measurements of $CO_2$ in gas and seawater at equilibrium. Mar. Chem. **70**: 105–119. https://doi.org/10.1016/S0304-4203(00)00022-0

McLeod, E. G. L. Chmura, S. Bouillon, R. Salm, M. Björk, C. M. Duarte, C. E. Lovelock, W. H. Schlesinger, and B. R. Sillman. 2011. A blueprint for blue carbon: toward an improved understanding of the role of vegetated coastal habitats in sequestering $CO_2$. Front. Ecol. Environ. **9**: 552–560. https://doi.org/10.1890/110004

Millero, F. J. 2007. The Marine Inorganic Carbon Cycle. Chem. Rev. **107**: 308–341. https://doi.org/10.1021/cr0503557

Mucci, A. 1983. The solubility of calcite and aragonite in seawater at various salinities, temperatures, and one atmosphere total pressure. Am. J. Sci. **283**: 780–799. https://doi.org/10.2475/ajs.283.7.780

Orr, J. C., J.-M. Epitalon, A. G. Dickson, and J.-P. Gattuso. 2018. Routine uncertainty propagation for the marine carbon dioxide system. Mar. Chem. **207**: 84–107. https://doi.org/10.1016/j.marchem.2018.10.006

Parra, S. M., and others. 2020. Bonnet Carré Spillway freshwater transport and corresponding biochemical properties in the Mississippi Bight. Cont. Shelf Res. **199**: 104114. https://doi.org/10.1016/j.csr.2020.104114

Perez, F. F. and F. Fraga. 1987. Association constant of fluoride and hydrogen ions in seawater. Mar. Chem. **21**: 161–168. https://doi.org/10.1016/0304-4203(87)90036-3

Peterson, R. N., W. S. Moore, S. L.Chappel, R. F. Viso, S. M. Libes, L. E. Peterson. 2016. A new perspective on coastal hypoxia: the role of saline groundwater. Mar. Chem. **179**: 1–11. https://doi.org/10.1016/j.marchem.2015.12.005

Pierrot, D. E. Lewis, and D. W. R. Wallace. 2006. MS Excel Program Developed for CO2 System Calculations. ORNL/CDIAC-105a. Carbon Dioxide Information Analysis Center, Oak Ridge National Laboratory, U.S. Department of Energy, Oak Ridge, Tennessee. doi: 10.3334/CDIAC/otg.CO2SYS_XLS_CDIAC105a

Pilson, M. E. Q. 2014. Changing pH in the surface ocean. Oceanogr. **27**: 120–125. https://doi.org/10.5670/oceanog.2014.15

Posadas, B. C. 2019. Economic impacts of coastal hazards on Mississippi commercial oyster fishery from 2005 to 2016. J Ocean Coastal Econ. **6**: https://doi.org/10.15351/2373-8456.1115

Ries, J. B., M. N. Ghazaleh, B. Connolly, I. Westfield, K. D. Castillo. 2016. Impacts of seawater saturation state ($\Omega_A$= 0.4–4.6) and temperature (10, 25°C) on the dissolution kinetics of whole–shell biogenic carbonates. Geochim. Cosmochim. Acta **192**: 318–337.

Rodellas, V., J. Garcia-Orellana, P. Masqué, M. Feldman, Y. Weinstein. 2015. Submarine groundwater discharge as a major source of nutrients to the Mediterranean Sea. Proc. Natl. Acad. Sci. Unit. States Am. **112**, 3926–3930. https://doi.org/10.1073/pnas.1419049112

Sanial, V., A. M. Shiller, D. Joung, and P. Ho. 2019. Extent of Mississippi River water in the Mississippi Bight and Louisiana Shelf based on water isotopes. Estuar. Coast. Shelf S. **226**: 106196. https://doi.org/10.1016/j.ecss.2019.04.030

Schroeder, W. W. 1978. Riverine influence on estuaries: a case study, p. 347–364. *In* Estuarine Interactions. Academic Press.

Schroeder, W. W., S. P. Dinnel, and W. J. Wiseman. 1990. Salinity stratification in a river–dominated estuary. Estuaries **13**: 145–154.

Shiller, A. M. 2003. Syringe filtration methods for examining dissolved and colloidal trace element distributions in remote field locations. Environ. Sci. Technol. **37**: 3953–3957.

Shumway, S. E. 1996. Chapter 13: Natural Environmental Factors, p. 467–513. *In* Kennedy, V. S., R. I. E. Newell, and A. F. Eble [eds.], The eastern oyster: *Crassostrea virginica*. Md. Sea Grant Publ.

Sikora, W. B. and B. Kjerfve. 1985. Factors influencing the salinity regime of Lake Pontchartrain, Lousiana, a shallow coastal lagoon: Analysis of a long-term data set. Estuaries **8**: 170–180.

Strickland, J. D. H. and T. R. Parsons. 1972. A practical hand book of seawater analysis. J. Fish. Res. Board Can. **157**: 49–70.

Sutton, A. J., R. A. Feely, S. Maenner-Jones, S. Musielwicz, and J. Osborne. 2019. Autonomous seawater $pCO_2$ and pH tie series from 40 surface buoys and the emergene of anthropogenic trends. Earth. Syst. Sci. Data **11**: 421–439. https://doi.org/10.5194/essd-11-421-2019

U.S. Geological Survey. 2016. National Water Information System data available on the World Wide Web (USGS Water Data for the Nation), accessed [May 10, 2020], at URL [http://waterdata.usgs.gov/nwis/].

Vinogradov, S., N. T. Vinogradova, V. Kamenkovich, and D. Nechaev. 2004. Temperature and Salinity Variability in the Mississippi Bight. Mar. Technol. Soc. J. **38**: 52–60. https://doi.org/10.4031/002533204787522433

Wang, Z. A., R. Wanninkhof, W. J. Cai, R. H. Byrne, X. Hu, T. H. Peng, and W. J. Huang. 2013. The marine inorganic carbon system along the Gulf of Mexico and Atlantic coasts of the United States: Insights from a transregional coastal carbon study. Limnol. Oceanogr. **58**: 325–342.

Wanninkhof, R. 1992. Realtionship between wind speed and gas exchange over the ocean. J. Geophys. Res. **97**: 7373–7382.

Wanninhkof, R. and W. R. McGillis. 1999. A cubic relationship between air–sea $CO_2$ exchange and wind speed. Geophys. Res. Lett. **26**: 1889–1892.

Weiss, R. F. 1974. Carbon dioxide in water and seawater: the solubility of a non–ideal gas. Mar. Chem. **2**: 203–215.

Weiss, R. F. and B. A. Price. 1980. Nitrous oxide solubility in water and seawater. Mar. Chem. **8**: 347–359.

Xue, Z., R. He, K. Fennel, W. J. Cai, W. Huang, H. Tian, and Z. Zang. 2016. Modeling $pCO_2$ variability in the Gulf of Mexico. Biogeosciences **13**: 4359–4377.

Yang, B., R. H. Byrne, M. Lindemuth. 2015. Contributions of organic alkalinity to total alkalinity in coastal waters: a spectrophotometric approach. Mar. Chem. **176**: 199–207.